ELSEVIER

Contents lists available at ScienceDirect

Acta Materialia

journal homepage: www.elsevier.com/locate/actamat



Full length article

Dislocation formation in the heteroepitaxial growth of PbSe/PbTe systems

Yang Li^{a,*}, Boyang Gu^a, Adrian Diaz^b, Simon R. Phillpot^c, David L. McDowell ^{d,e}, Youping Chen^a

- ^a Department of Mechanical and Aerospace Engineering, University of Florida, Gainesville, FL 32611, USA
- ^b X-Computational Physics Division, Los Alamos National Laboratory, P.O. Box 1663, Los Alamos, NM, USA
- ^c Department of Materials Science and Engineering, University of Florida, Gainesville, FL 32611, USA
- d Woodruff School of Mechanical Engineering, Georgia Institute of Technology, Atlanta, GA 30332, USA
- ^e School of Materials Science and Engineering, Georgia Institute of Technology, Atlanta, GA 30332, USA

ARTICLE INFO

Keywords: Heteroepitaxial growth Dislocation formation Misfit dislocation Threading dislocation

Multiscale simulation

ABSTRACT

The paper presents a multiscale study of the kinetic processes of the heteroepitaxial growth of the PbSe/PbTe (111) and PbTe/PbSe(001) systems, using the Concurrent Atomistic-Continuum (CAC) method as the simulation tool. The CAC simulations have reproduced the Stranski-Krastanov growth mode and the layer-by-layer growth mode of the two systems, respectively; the pyramid-shaped island morphology of the PbSe epilayer on PbTe (111), the square-like misfit dislocation networks within the PbTe/PbSe(001) interface, and the critical thickness for the PbTe/PbSe(001) system at which coherent interfaces transit to semi-coherent interfaces with the formation of misfit dislocations, all in good agreement with experimental observations. Four types of misfit dislocations are found to form during the growth of the two PbTe/PbSe heterosystems, and hexagonal-like misfit dislocation networks are observed within the PbSe/PbTe(111) interfaces. The growth processes, including the formation of misfit dislocations, have been visualized. Dislocation half-loops have been observed to nucleate from the epilayer surfaces. These half-loops extend towards the interface by climb or glide motions, interact with other half-loops, and form misfit dislocation networks at the interfaces and threading dislocations extending from interfaces to epilayer surfaces. The dominant types of misfit dislocations in both systems are found to be those with Burgers vectors parallel to the interfaces, whereas the misfit dislocations with Burgers vectors inclined to the interface have a low likelihood of generation and tend to annihilate. The size of the substrate is demonstrated to have a significant effect on the formation, evolution, and distribution of dislocations on the growth of PbSe on PbTe(111).

1. Introduction

A fundamental structure of semiconductor devices is the multilayered heterostructure. The most widely used bottom-up method for fabricating semiconductor multilayered heterostructure is heteroepitaxy, in which a crystalline epilayer grows on a substrate or a film of a different crystalline material. Defects, such as misfit and threading dislocations, have been widely observed in such epitaxial heterostructures. These dislocations significantly influence the functionalities of the systems, as they induce electron scattering that reduces carrier mobility and increases current leakage path[1,2]. They also scatter phonons, leading to device self-heating, and consequently significantly limit the performance of the devices[3].

Extensive theoretical and experimental efforts have been devoted to

the understanding of the formation of defects during heteroepitaxial growth since the 1940s[4–9]. These theoretical and experimental studies have firmly established the following.

- Misfit dislocations are the ubiquitous defects in strained heterostructures and there is a critical thickness during the heteroepitaxial growth of an epilayer; above this layer thickness, formation of misfit dislocations and concomitant threading dislocations are unavoidable, regardless of the growth mechanism or growth conditions [4–10].
- 2) This critical thickness depends not only on the lattice mismatch but also on the growth area and substrate size[11].
- The structure and density of the dislocations in the epitaxial heterostructures vary with structural parameters, such as the epilayer

E-mail address: yangli1991@ufl.edu (Y. Li).

^{*} Corresponding author.

thickness[12], and kinetic parameters, such as the growth temperature[13].

Despite extensive theoretical and experimental efforts, our understanding of the underlying mechanism for misfit and threading dislocation formation remains limited. State-of-the-art experimental techniques are unable to provide a direct observation of the nucleation of dislocations and their evolution in space and time at sufficiently resolved length or time scales. Various theories have been proposed to predict the critical thickness for misfit dislocation formation at the interface between the epilayer and the substrate, including the Frank and van der Merwe (FM) method derived from the energy balance between the strain energy and the interface energy[4], the Matthews and Blackeslee (MB) method derived based on forces acting on an existing dislocation due to elastic stress in the system[8], and the modified MB by People and Bean by considering dislocation nucleation at the interface [14]. Discrepancies between theoretical predictions and experimental measurements have been reported, as these theories do not include the kinetics of dislocation nucleation or different dislocation nucleation mechanisms in different materials systems or growth conditions.

Computational approaches hold promise to complement experimental techniques by providing details regarding the kinetic processes of heteroepitaxial growth. Among various computational approaches that have attempted to understand the formation of dislocations during heteroepitaxial growth, e.g., molecular dynamics[15] (MD) and the kinetic Monte Carlo method[16], or to reproduce the morphological evolution of the epitaxial film, e.g., the phase field model [17], MD is the only method that does not require a priori assumptions about the mechanisms related to growth, such as growth mode, or to defects, such as defect structures and formation mechanisms. Over the past few decades, various MD simulations have sought understanding of the kinetic processes of dislocation formation and the underlying mechanisms. For example, in 1997 Dong et al. performed MD simulations of the growth of two-dimensional systems based on a Lennard-Jones potential and investigated the mechanisms for dislocation nucleation in tension and compression conditions [15]; in 2006, Zhou et al. used MD to investigate the epitaxial growth of FCC aluminum on a strained aluminum substrate [18] and proposed a "fusion-crystallization mechanism for nucleation of misfit dislocations"; in 2016, Jose Chavez et al. performed MD simulations of CdTe growth on CdS and demonstrated the dependence of dislocation morphology on substrate orientation[19]; in 2017, Gruber et al.[20] simulated the growth of InGaN on a GaN (0001) substrate using MD and quantified the influence of growth temperature and growth rate on dislocation formation. These efforts have provided insights into the formation of dislocations. However, none of these MD simulations have reproduced the experimental observed dislocation networks or the substrate size-dependent critical thickness. Such mesoscale aspects have eluded MD.

The chief limitation of MD is its very small length and time scales. In the aforementioned MD growth simulations, the largest model contains ~1 million atoms with the thickness of the substrate being limited to a few nanometers to a few tens of nanometers. However, the smallest systems studied in experiments have meso- or macro-scale (100 nm to 100 mm) substrates. Moreover, experimental studies have demonstrated a significant effect of the substrate size and deformation on the critical thickness, especially for those systems that follow the Stranski-Krastanov (SK) growth mode, such as Ge/Si (001)[11] and InGaAs/-GaAs (100)[21,22], which suggests that predicting the dislocation structure and density in heteroepitaxial growth, or identifying the generation mechanisms of dislocations, requires a mesoscale modeling method with sufficient predictive character.

This work aims to address the length scale challenge for simulations of heteroepitaxial growth by using a multiscale method, i.e., the Concurrent Atomistic-Continuum (CAC) method[23]. The goal is to investigate the formation of misfit and threading dislocations during heteroepitaxial growth, provide information regarding the atomic-scale

kinetic processes, and quantify the effect of the size of the substrate. CAC is an atomic interaction-based multiscale method[23-25]. It builds on the formulation that extends Irving and Kirkwood's statistical mechanical theory of transport processes for homogenized systems[26] to polyatomic crystalline systems with a concurrent atomic and continuum description of the structure of all crystals. It reduces the degrees of freedom (DOFs) of an atomistic system by utilizing the continuous structure and dynamics of single crystals at the lattice level, while preserving the discrete atomic structure and motion within each lattice cell. Consequently, the CAC conservation equations and flux formulae are valid at multiple length and time scales ranging from the atomic scale to the macroscale[27-29]. The CAC formulation is numerically implemented in the LAMMPS codebase employing a modified finite element method[23]. By concurrently modeling a system with atoms and finite elements under one consistent set of governing equations, CAC can go beyond MD to study mesoscale systems. The main advantage of CAC for simulations of heteroepitaxial growth is that the meso or macro-scale substrates can be modeled with coarse-meshed finite elements (FEs). while the growth of the epilayer can be simulated with full atomic resolution. Similar to MD, CAC needs no assumptions of the mechanisms or materials parameters regarding the growth process other than an interatomic potential. The applicability of CAC in predicting dynamic material behaviors or processes, such as crack initiation and branching [30,31], phase transitions[32], dislocation nucleation[33-36], loop formation[37-40] and interactions with other defects[41-47], or phonon-dislocation[48-50], phonon-interface[51], and phonon-internal surface interactions[52], has been verified through one-to-one comparisons with MD simulations.

We choose PbTe/PbSe(100) and PbSe/PbTe(111) heterosystems for this study for several reasons. First, the PbSe-PbTe heterostructurebased system is one of today's most efficient thermoelectric materials [53,54]; it also has important applications in infrared devices[55,56]. Second, there is a well-developed interatomic potential that can reproduce the thermal and mechanical properties of PbTe/PbSe systems reasonably well[50,57]. Third, there are consistent experimental observations and data for the heteroepitaxial growth of the PbTe/PbSe (100) and PbSe/PbTe (111) systems[58-64]. Specifically, on a PbSe (100) substrate, the PbTe epilayer has been reported to grow in a layer-by-layer growth mode, and square-shaped misfit dislocation networks (dislocation alignment along <110> directions) have been observed to form at the interfaces[59,61]. Meanwhile, on a PbTe(111) substrate, the PbSe epilayer has been observed to grow in the SK growth mode (i.e., layer-by-layer growth followed by island growth); the PbSe islands have been found to have pyramidal shapes with triangular bases and {100} side facets[62,63]; the misfit dislocations within the PbSe/PbTe(111) interface have been observed to have alignment along <110> directions[64]. The existing experimental results facilitate direct comparison with our simulation results. Fourth, the heteroepitaxial growth of PbTe/PbSe (100) and PbSe/PbTe (111) systems has not yet been studied using any computational methods, and a fundamental understanding of the kinetic processes of dislocation formation in the two systems, as well as the underlying mechanisms, remains limited.

The paper is organized as follows. In Section 2, we introduce the simulation methodology, including the computational models and details of the simulation setup, and conduct a comparison of the CAC simulation results with MD simulation results to quantify the accuracy and efficiency of the CAC method with respect to MD. In Section 3, we present CAC simulation results of the kinetic processes of dislocation nucleation, interaction, and annihilation during the growth processes, the effect of the substrate size, and the underlying mechanisms. This paper concludes with a brief summary and discussion in Section 4.

2. Methodology

2.1. Computer models and simulation setup

This work focuses on the deposition processes in molecular beam epitaxy of two systems: the growth of PbSe on PbTe(111) substrate and the growth of PbTe on PbSe(100) substrate. In Fig. 1, we present a schematic cross-sectional view of the mesh used in the CAC model for heteroepitaxy. A 3-nm top layer of the substrates is modeled with atomic resolution, while the rest of the substrate is discretized into coarse-scale finite elements (FEs) with element size changing gradually from 4 \times 4 \times 4 unit cells per element to 16 \times 16 \times 16 unit cells per element as the distance between the element and the substrate top surface increases. All the FEs have the rhombohedral shape with each node containing a primitive unit cell of the PbTe or PbSe crystal.

The substrate in each simulation is first heated to the growth temperature by rescaling the velocities of the atoms and the FE nodes in the substrate. The growth process is simulated by continuously injecting Pb and Se atoms (or Pb and Te atoms) onto the substrate surface from random locations above the substrate, with the Pb:Se (or Pb:Te) flux ratio of 1:1 and the kinetic energy of each atom of 0.1 eV. The overall growth rate ranges from 0.1 monolayer (ML) per nanosecond to 0.4 ML per nanosecond. A reflect-particle boundary is set 50 nm above the substrate surface to prevent atoms from flying out of the top boundary of the simulation box. The atoms that attempt to move through the reflectparticle boundary from the bottom up will be reflected back. A free boundary condition is applied along the Z direction. Periodic boundary conditions are applied along X and Y directions. A small viscous damping force is applied to the FE region and the bottom of the atomic region of the substrate when the substrate temperature rises above the designated growth temperature. As a result, the substrate temperature is maintained around the designated growth temperature throughout the entire growth process, which ranges from 650 K to 900 K, depending on the specific simulation. Note that there is no viscous damping force applied to the surface region of the substrate or the epilayer. Thus, the evolution of the epilayer and the defects in the epilayer or at the substrate/epilayer interface are not affected by the damping.

The growth temperatures in the experiments of both systems are 650 K and the growth rates are typically 0.08-0.4 ML/s, depending on specific experiments[61–63]. To quantify the effects of growth rate, we performed simulations with different growth rates (0.1 ML/ns - 0.4

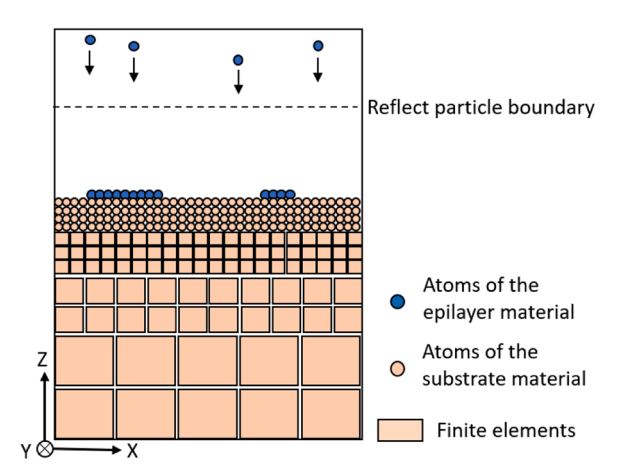


Fig. 1. A schematic cross-sectional view of a CAC model for growth simulations. The top surface region of the substrate is modeled using atomic resolution. The rest domain of the substrate is modeled using coarse-scale finite elements. The X, Y, and Z directions are along the $[\overline{1}10]$, $[\overline{1}\overline{1}2]$ and [111] lattice directions of the PbSe/PbTe(111) system, while along the [100], [010], and [001] lattice directions of the PbTe/PbSe(100) systems. The Z direction is the growth direction.

ML/ns) for several different growth temperatures (650 K - 900 K). Simulation results show that the two systems behave differently. For the PbSe/PbTe(111) system, both the critical thickness for dislocation nucleation and the dislocation density are affected by the growth rate, and more defects such as voids form at higher growth rates. This effect, however, decreases with increasing growth temperature. Therefore, a relatively higher growth temperature, 900K, is used for the PbSe/PbTe (111) system. It is noted that employment of higher growth temperature is commonly used to mitigate the effect of high growth rates in simulations, as the growth rates in experiments (on the order of ML/s) are several orders lower than those in simulations [20,65,66]. By contrast, for the PbTe/PbSe(001) system, the results of the growth processes, including the critical thickness and dislocation density, are not significantly affected by the growth rate within the range tested. Therefore, the experimental growth temperature of 650 K is employed in all the growth simulations of the PbTe/PbSe(001) system.

To quantify the effect of the substrate size, a series of CAC models were built with the substrate dimensions ranging from $50\times50\times10~\text{nm}^3$ to $200\times200\times200~\text{mm}^3$. The largest substrate contains 84K elements and 4.8 million atoms. An MD model for the substrate with the same size would contain $\sim\!260$ million atoms, which is several hundred times larger than the largest MD models for growth simulations to date, while the largest CAC models only have $\sim\!2.4\%$ of the DOFs of the corresponding MD model. Moreover, since the top surface region of the substrate and the epilayer are atomically resolved, CAC simulations are able to accurately capture the evolution of the epilayer, the nucleation and evolution of misfit and threading dislocations, as well as the atomic-scale core structures of the dislocations, during the kinetic processes of the growth.

An interatomic potential that consists of long-range Coulombic potential and short-range Buckingham potential[57] is employed to describe the interaction among Pb, Te, and Se atoms in the simulations. The Coulombic interactions are computed via the damped shifted force method[67]. The potential is built on the transferrable potential for CdTe-CdSe-PbSe-PbS system[68]. The relative stability (energies) of different phases and surface energies of PbTe and PbSe are included in the training set of the interatomic potential, enabling the potential to capture the transformation between compound phases and to simulate crystalline growth [66,68]. The accuracy of the potential in reproducing the lattice constants, elastic properties, and phonon dispersion relations [50] of PbTe and PbSe has been quantified by comparing to density functional theory (DFT) calculation results. The potential has also been demonstrated to be capable of reproducing the misfit dislocation network within the PbTe/PbSe(100) interface[50] in excellent agreement with experimental observations[59-61].

2.2. Comparisons between CAC and MD simulation results

To quantify the accuracy of CAC simulations with respect to MD, we compare the CAC and MD simulation results of the growth processes of PbSe on PbTe(111) and PbTe on PbSe(001), respectively. A small substrate with dimensions of 50nm×50nm×10nm is used for both systems in order for MD to simulate the kinetic processes. The number of DOFs of the CAC models is about 36% of that of the MD models for the small models. It is noticed that the largest system studied in this work has substrate dimensions of 200nm×200nm×200nm, and the DOFs of the CAC model of the system are \sim 2.4% of the corresponding MD model. In Fig. 2, we compare the results of the dislocation densities at different stages of growth (Figs. 2a and 2c) and the dislocation networks in the two systems at different epilayer coverages (Figs. 2b and 2d). OVITO DXA (Dislocation Extraction Algorithm)[69] is employed to analyze and present the dislocation networks in the systems through line-based representations. As can be seen from Fig. 2, the CAC simulation results of the dislocation networks, as well as the dislocation density, agree very well with those obtained by MD. This excellent agreement demonstrates that, with significantly reduced DOFs, CAC can reproduce the

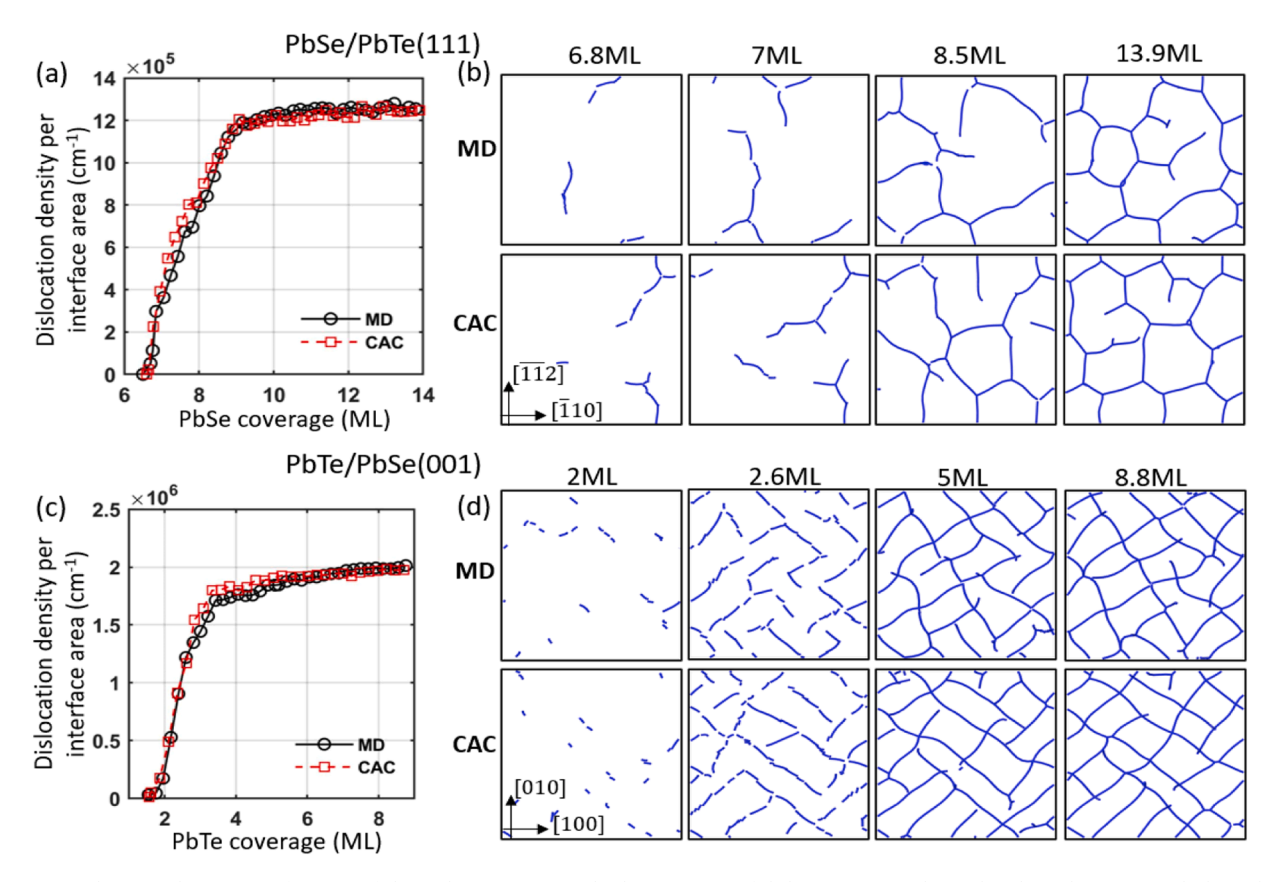


Fig. 2. (a, c) Dislocation density as a function of the epilayer coverage. (b, d) Top views of dislocation networks in the PbSe/PbTe(111) and PbTe/PbSe(001) heteroepitaxial structures with different epilayer coverages, obtained from CAC and MD simulations, visualized using OVITO DXA.

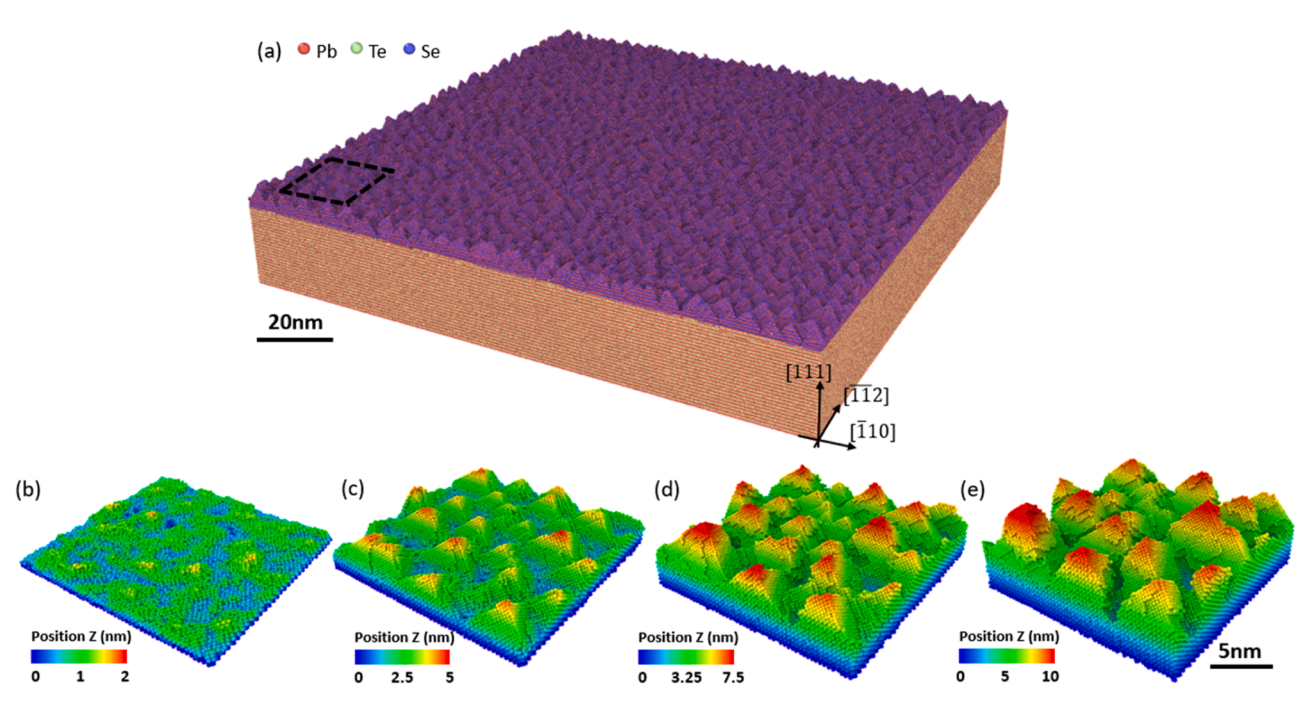


Fig. 3. (a) Perspective view of atomic positions of the PbSe/PbTe(111) epitaxial heterostructure obtained from CAC simulations. Only the epilayer and the top region of the substrate are displayed. (b-e) Zoomed-in views of the PbSe epilayer in the region marked by the dashed square in (a) at (b) 3 ML, (c) 7.5 ML, (d) 11.9 ML, and (e) 16.8 ML coverages. In (b-e), atoms are colored according to their positions along the Z direction with respect to the interface.

dislocation structures and densities in PbSe/PbTe(111) and PbTe/PbSe (001) heteroepitaxial structures that would be obtained by MD.

3. Simulation results

3.1. Surface morphology of epilayers and growth modes

In Figs. 3 and 4, we present the CAC simulation results of the atomic positions of the PbSe/PbTe(111) and PbTe/PbSe(001) heteroepitaxial structures. All simulation results presented in this paper are from CAC simulations of the growth processes on the 200×200×200 nm³ substrates, unless stated otherwise. As can be seen from Figs. 3(b-e), the surface of the epilayer in the PbSe/PbTe(111) structure is relatively flat at 3 ML PbSe coverage, but becomes rough as the growth process continues. The root mean square (RMS) of the PbSe epilayer surface roughness gradually increases from 3.5 Å at 3 ML coverage to 20 Å at 16.8 ML coverage. It is seen from Figs. 3(c-e), the PbSe epilayer consists of pyramid-shaped islands with triangular bases and {100} side facets. This is consistent with the pyramid-shaped surface morphology of the PbSe epilayer observed in the experiments[62,63]. The evolution of the surface morphology indicates that the growth of PbSe on PbTe(111) follows the Stranski-Krastanov (SK) growth mode, also knowns as the "layer-plus-island growth mode", which is in correspondence with the experimental observation of heteroepitaxy of this system[62,63].

In contrast to PbSe/PbTe(111), the surface of the PbTe epilayer in the PbTe/PbSe(001) structure is relatively flat and smooth during the growth simulations, as shown in Fig. 4. The RMS surface roughness of the PbTe epilayer surface is around 2.5 Å, smaller than the thickness of a 1 ML PbTe thin film which is around 3 Å. The growth process of PbTe on PbSe(001) is shown to follow the layer-by-layer growth mode, in agreement with the experimental observations for this system[61]. The different growth modes along (111) and (001) growth orientations can be explained by the relationship between the free surface energy and the strain energy, as well as the fact that the (001) surface in PbTe or PbSe has the lowest free surface energy. In the (111) growth orientation, islands with {001} side facets are preferred to form, as the reduction of strain energy due to island formation outweighs the increase in free

surface energy[63]. Meanwhile, for the (001) growth orientation, islands do not form because the additional surface energy required is larger than the strain energy that can be reduced from the island formation[61]. The agreement with the experimental observations in the evolution of the epilayer surface morphology indicates that CAC simulations are able to capture the essential features of the physical processes of the heteroepitaxial growth of the two PbTe/PbSe heterosystems.

3.2. Dislocation structures

OVITO DXA is used to analyze the dislocation structures and their evolutions during epitaxial growth. It is observed that in both systems, dislocations are nucleated from the epilayer surfaces, extend to the interfaces, and form misfit and threading dislocations. The dislocation structures in the PbSe/PbTe(111) structure at 16.8 ML PbSe coverage and the PbTe/PbSe(001) structure at 16.1 ML PbTe coverage are presented in Figs. 5 and 6, respectively; the formation mechanisms of the misfit and threading dislocations will be discussed in Section 3.3.

As can be seen from Figs. 5(a) and 5(b), the dislocation network in the PbSe/PbTe(111) heterostructure consists of 1/2<110>(111) and 1/ 2<110>{100} dislocations, shown as blue and red lines in Fig. 5(a) and 5(b). In Fig. 5(c), we present the atomic structures of the 1/2 < 110 >(111) and 1/2<110>{100} misfit dislocations, both of which are edge dislocations. The 1/2<110>(111) misfit dislocations have Burgers vectors parallel to the PbSe/PbTe(111) interface, while the 1/2<110> {100} dislocations have Burgers vectors inclined to the PbSe/PbTe(111) interface. As can be seen from Fig. 5(c), the substrate is not flat, indicting the deformation of the substrate, which will be discussed further in Section 3.4. Based on calculations of dislocation lengths from the simulation results, misfit dislocations make up 86% of all the dislocations in the structure and the 1/2<110>(111) misfit dislocations account for 90.3% of all the misfit dislocations in the structure. This indicates that the 1/2 < 110 > (111) misfit dislocations are the main type of dislocations in the PbSe/PbTe(111) heterostructure.

In Figs. 6(a) and 6(b), we present the top and side views of the dislocation networks in the PbTe/PbSe(001) heterostructure at 16.1 ML PbTe coverage. The experimental results[61] are also presented in Fig. 6

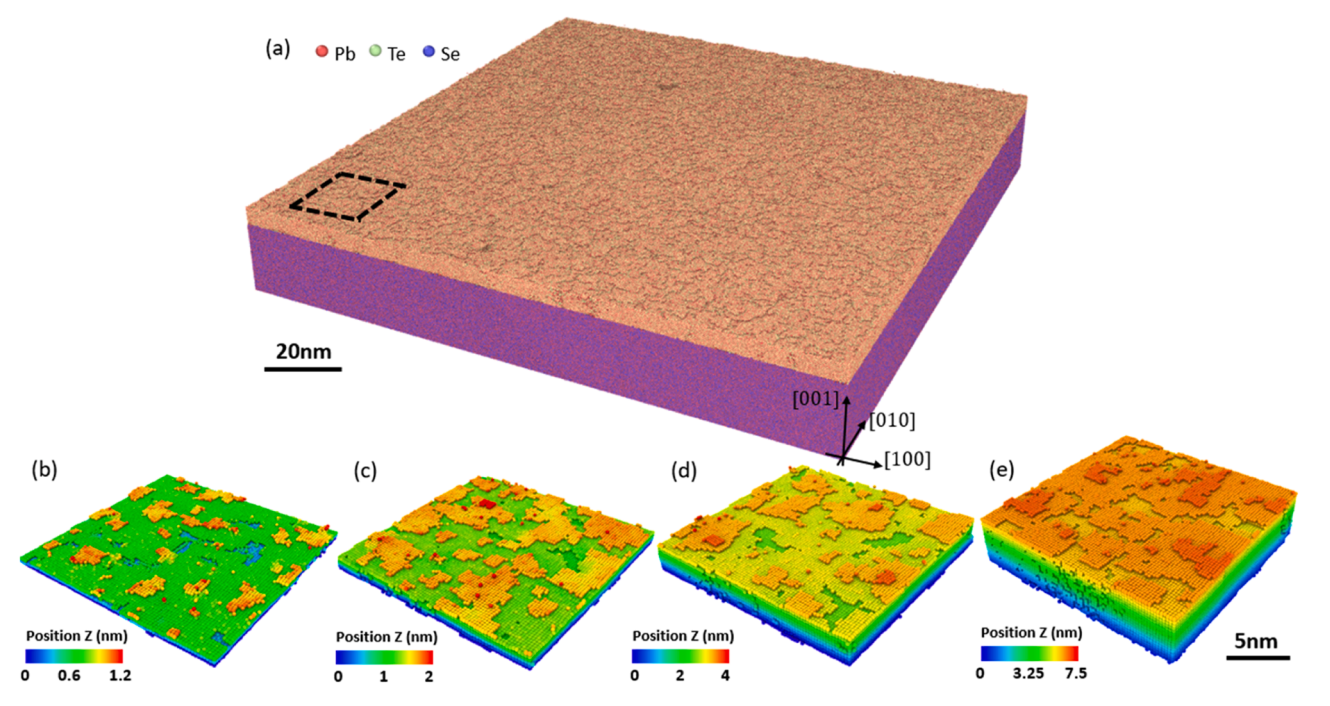


Fig. 4. (a) Perspective view of atomic positions of the PbTe/PbSe(001) epitaxial heterostructure obtained from CAC simulations. Only the epilayer and the top region of the substrate are displayed. (b-e) Zoomed-in views of the PbTe epilayer in the region marked by the dashed square in (a) at (b) 2 ML, (c) 4 ML, (d) 8.5 ML, and (e) 16.1 ML coverages. In (b-e), atoms are colored according to their positions along the Z direction with respect to the interface.

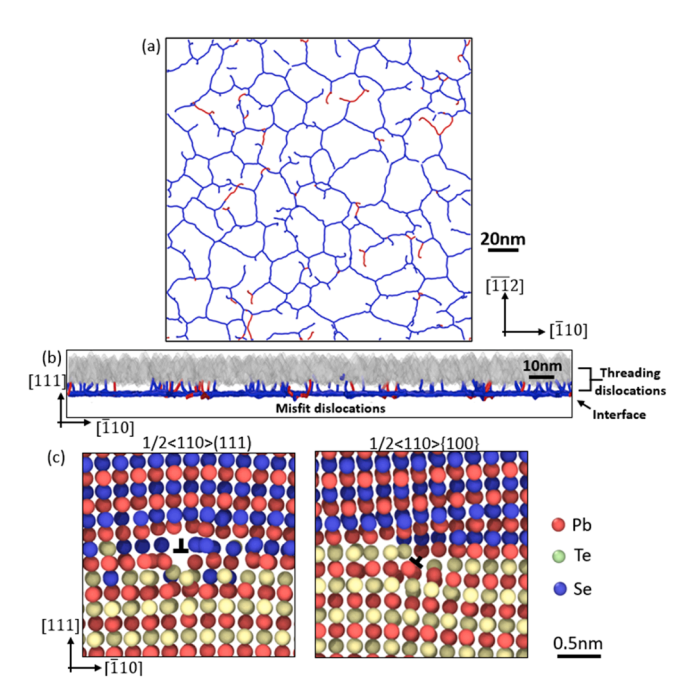


Fig. 5. (a) Top and (b) side views of dislocation networks in the PbSe/PbTe (111) heterostructure at 16.8 ML PbSe coverage, visualized using OVITO DXA. Blue lines represent 1/2 < 110 > (111) dislocations. Red lines represent 1/2 < 110 > (100) dislocations. (c) Atomic structures of 1/2 < 110 > (111) and 1/2 < 110 > (100) misfit dislocations.

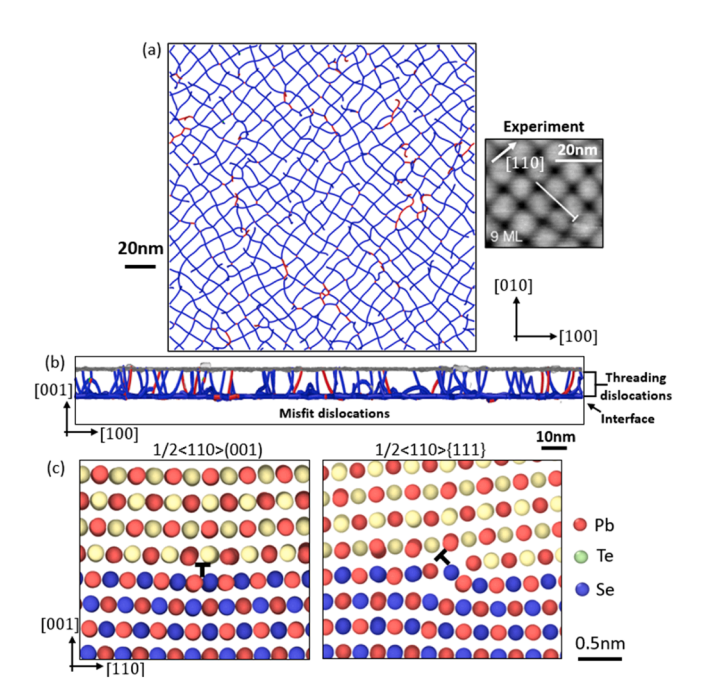


Fig. 6. (a) Top and (b) side views of dislocation networks in the PbTe/PbSe (001) heterostructure at 16.1 ML PbTe coverage, visualized using OVITO DXA. Blue lines represent 1/2 < 110 > (001) dislocations. Red lines represent 1/2 < 110 > (111) dislocations. (c) Atomic structures of 1/2 < 110 > (001) and 1/2 < 110 > (111) misfit dislocations. A scanning tunneling microscopy image of PbTe epilayers on PbSe(001) at a coverage of 9 ML from the experiments (adapted from the figure in ref.[61]) is presented in (a) for comparison.

(a) for comparison purposes. The dislocation network in the PbTe/PbSe (001) heterostructure is shown to consist of 1/2 < 110 > (001) and $1/2 < 110 > \{111\}$ misfit and threading dislocations. As can be seen from the atomic structures presented in Fig. 6(c), both types of misfit

dislocations are edge dislocations, with the 1/2<110>(001) misfit dislocations having Burgers vectors parallel to the interface, and the $1/2<110>\{111\}$ misfit dislocations having Burgers vectors inclined to the interface. Based on calculations of dislocation lengths from the simulation results, 90.4% of dislocations in the PbTe/PbSe(001) heterostructure are misfit dislocations, and 94.7% of misfit dislocations are 1/2<110>(001) misfit dislocations. Thus, the 1/2<110>(111) misfit dislocations are the main type of dislocations in the PbTe/PbSe(001) heterostructure.

The 1/2<110>(111) and 1/2<110>(001) misfit dislocations are more prevalent in the PbSe/PbTe(111) and PbTe/PbSe(001) heterostructures, respectively. This is because their Burgers vectors are parallel to the PbSe/PbTe(111) and PbTe/PbSe(001) interfaces, and therefore they are able to most efficiently relieve the lattice mismatch strain in the two systems, resulting in the lowest energy state. Also, as can be seen from Figs. 5(a) and 6(a), the misfit dislocation networks in the two PbTe/PbSe heterostructures exhibit hexagonal-like and square-like shapes, respectively. This is because that 1/2<110>(111) and 1/ 2<110>(001) misfit dislocations are the main types of dislocations in the two systems and the orientations of their Burgers vectors render them to have the hexagonal-like and square-like arrangements within the interfaces, as shown in Fig. 7. Additionally, it is seen from Figs. 5(a) and 6(a) that the hexagonal-like dislocation network in the PbSe/PbTe (111) structure is less uniform than the square-like dislocation network in the PbTe/PbSe(001) structure. This is due to the different mobilities of the 1/2<110>(111) and 1/2<110>(001) misfit dislocations within the interfaces and the substrate deformation, which will be discussed more in Section 3.3 and 3.4.

It is noted that both the atomic-scale dislocation core structures and the dislocation networks are obtained from CAC simulations of growth kinetics without any assumption of dislocation structures. They are consistent with experimental observations. Specifically, the square-like misfit dislocation network obtained from the simulation of the PbTe/PbSe(001) system agrees reasonably well with the experimental observations by Springholz and Wiesauer[61], as shown in Fig. 6(a). Additionally, the alignment of misfit dislocations along <110> directions obtained from the simulation of the PbSe/PbTe(111) system agrees well with the experimental observation by Takayanagi et al.[64].

3.3. Formation, interaction, and annihilation mechanisms of dislocations

3.3.1. PbSe/PbTe(111)

In Fig. 8 we present the simulation results of the dislocation density as a function of the PbSe coverage and the evolution of dislocation networks in the PbSe/PbTe(111) heterostructure. The dislocation density is calculated based on the ratio between the total length of dislocations and the interface area. The critical thickness of the PbSe epilayer for dislocation nucleation is 7.5 ML. During the growth of the PbSe epilayer from 7.5 ML to 10 ML coverage, the dislocation density increases rapidly from 0 to $6.2\times10^5~\rm cm^{-1}$. A number of small dislocation

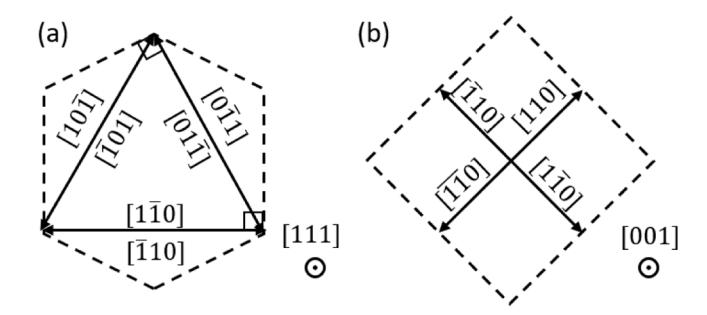


Fig. 7. Possible Burgers vectors (arrows) and dislocation lines (dashed lines) of (a) 1/2 < 110 > (111) dislocations in the PbSe/PbTe(111) system and (b) 1/2 < 110 > (001) dislocations in the PbTe/PbSe(001) system.

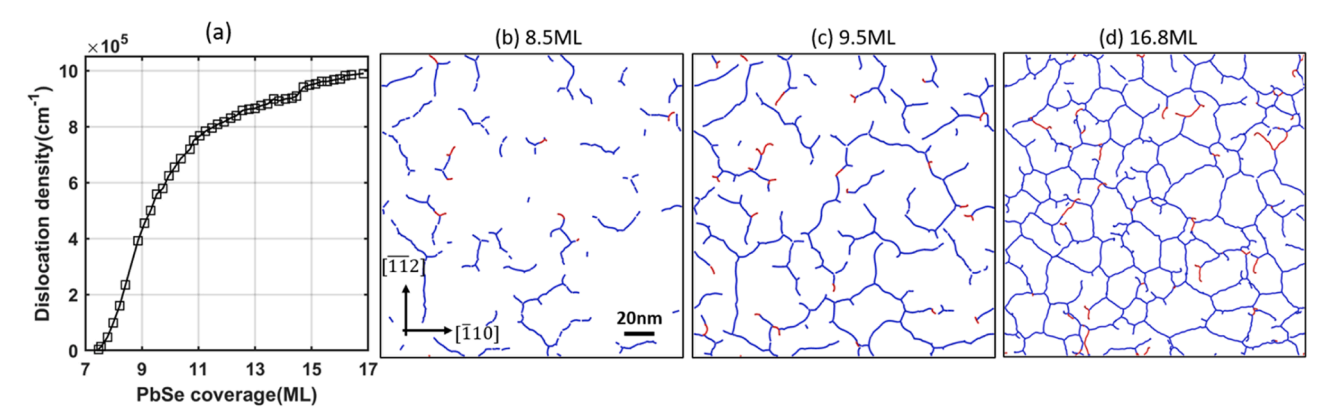


Fig. 8. (a) Dislocation density as a function of the epilayer coverage during the growth of PbSe on the PbTe(111) substrate with dimensions of $200 \times 200 \times 200 \text{ nm}^3$. (b-d) Top views of dislocation networks in the PbSe/PbTe(111) heterostructure at different PbSe coverages. Blue and red lines denote 1/2 < 110 > (111) and 1/2 < 110 > (100) dislocations, respectively.

half-loops nucleate at the epilayer surface. Subsequently, the dislocation density only increases by $3.7\times10^5~{\rm cm}^{-1}$ in the following 6.8 ML growth. At this stage, most lattice mismatch strain has been relieved by the three-dimensional islands in the epilayer and the dislocations formed previously. As a result, the rate of dislocation nucleation slows down. The threading dislocation density in the structure is also calculated based on the ratio between the number of threading dislocations and the interface area. At 16.8 ML PbSe coverage, the threading dislocation density is calculated to be $3.85\times10^{11}~{\rm cm}^{-2}.$

To identify the formation mechanism of misfit and threading dislocations in the PbSe/PbTe(111) heterostructure, we present a time sequence of the dislocations and their evolution in two zoomed-in regions of the PbSe/PbTe(111) epitaxial heterostructure in Figs. 9(a) and 9 (c), respectively. The atomic structures in the vicinity of the dislocations are presented in Figs. 9(b) and 9(d). As can be seen from Fig. 9(a), 1/ 2<110>(111) dislocation half-loops nucleate from the valleys of the pyramid-shaped epilayer surface. It is noted that the Burgers vectors and slip planes of the 1/2<110>(111) dislocations are parallel to the PbSe/ PbTe(111) interface. Thus, instead of glide motions, these dislocations extend towards the interface by virtue of vertical climb migration, which can be clearly seen from Fig. 9(b). The 1/2<110>(111) dislocation halfloops are also observed to merge with other dislocation half-loops in the same loop planes, forming larger dislocation half-loops, as shown in Fig. 9(a). As the dislocation half-loops reach the interface, they form the 1/2<110>(111) misfit dislocations and 1/2<110>(111) threading dislocations. The 1/2<110>(111) threading dislocation segments have edge-component Burgers vectors and are of edge and/or mixed types.

Fig. 9(c) presents the evolution process of a 1/2<110>{100} dislocation in a zoomed-in region of the PbSe/PbTe(111) structure from PbSe coverage of 11.1 ML to 12.3 ML, which shows that the $1/2 < 110 > \{100\}$ dislocation half-loop nucleate at the valley of the pyramid-shaped epilayer surface, similar to the 1/2<110>(111) dislocation half-loops. However, unlike the 1/2<110>(111) dislocations, which extend to the interface by climb or by merging with other dislocations, the 1/ 2<110>{100} dislocation extends to the interface by glide with its ends shifting among the valleys of the epilayer surface. This is because the 1/ 2<110>{100} dislocation has a Burgers vector inclined to the PbSe/ PbTe(111) interface, enabling it to glide along its slip plane towards the interface, as shown in Fig. 9(d). As the $1/2 < 110 > \{100\}$ dislocation halfloop glide to the interface, it generates a $1/2 < 110 > \{100\}$ misfit dislocation and two 1/2<110>{100} threading dislocations, as shown in Fig. 9(d). The 1/2<110>{100} threading dislocation segments have screw-component Burgers vectors and are of screw and/or mixed types.

It is noted that the dominant type of dislocations nucleated during the growth PbSe on the PbTe(111) substrates are 1/2 < 110 > (111) dislocations, which do not belong to the primary $< 110 > \{100\}$ slip systems. These dislocations extend to the interface through climb instead of glide.

This observation suggests that climb-type dislocations (i.e., 1/2 < 110 > (111) dislocations) are more likely to nucleate from the surface valleys than glide-type dislocations (i.e., $1/2 < 110 > \{100\}$ dislocations). This is consistent with the theoretical work by Gao[70], which suggested that there is a high nominal stress level at the valleys of the epilayer surface, making them extremely efficient sources of dislocation nucleation and that the problem of dislocation nucleation from surface valleys in heteroepitaxy is different from the conventional study of dislocation nucleation from a crack tip fixed in space. The constantly moving surface during the growth process provides a favorable condition for the nucleation of climb-type dislocations.

Our simulation results indicate that the 1/2<110>{100} misfit dislocations within the PbSe/PbTe(111) interface cannot glide within the interface and hence they are stationary. Consequently, their spatial distribution appears random and intermixed among the hexagonal-like networks of 1/2<110>(111) misfit dislocations, as shown in Fig. 8(d). It is also observed that the 1/2<110>{100} dislocations in the PbSe/ PbTe(111) heterostructure may annihilate during the growth process and generate 1/2<110>(111) dislocations. Fig. 10 shows the process of the annihilation of three 1/2<110>{100} dislocation segments, and the generation of a 1/2<110>(111) dislocation segment in the PbSe/PbTe (111) heterostructure. The three 1/2<110>{100} dislocation segments have the Burgers vectors of a/2[011], $a/2[\overline{1}0\overline{1}]$, and $a/2[\overline{1}0\overline{1}]$, respectively. As can be seen from Fig. 10, the three 1/2<110>{100} dislocation segments react and form a 1/2<110>(111) dislocation segment with the Burgers vector of $a/2[\overline{1}10]$. The process can be described by the reaction: $a/2[011] + a/2[\overline{1}0\overline{1}] \rightarrow a/2[\overline{1}10]$. This reaction reduces the potential energy of the system and hence is energetically favorable.

3.3.2. PbTe/PbSe(001)

Fig. 11 presents the CAC simulation results of the dislocation density as a function of the PbTe coverage and the evolution of dislocation networks in the growth of the PbTe/PbSe(001) heterostructure. The critical thickness of the PbTe epilayer for dislocation nucleation is 1.4 ML. It is slightly larger than the critical thickness of 1 ML observed in the experiments[61]. This discrepancy is a result of the inability of OVITO DXA to identify dislocations at the interface between a substrate and a very thin epilayer (\sim 1 ML), because the number of neighboring atoms is too small for an accurate analysis. During the early stage of the growth, the dislocation density increases rapidly, reaching 1.6×10^6 cm⁻¹ as the PbTe coverage increases from 1.4 ML to 3.3 ML. During this stage, small dislocation half-loops nucleate at the epilayer surface and merge with others. As the PbTe coverage continues to increase, the growth rate of dislocation density slows down, and dislocation density only increases by 5×10^5 cm⁻¹ from PbTe coverage of 3.3 ML to 16.1 ML. This indicates that at this stage most lattice mismatch strain has been accommodated

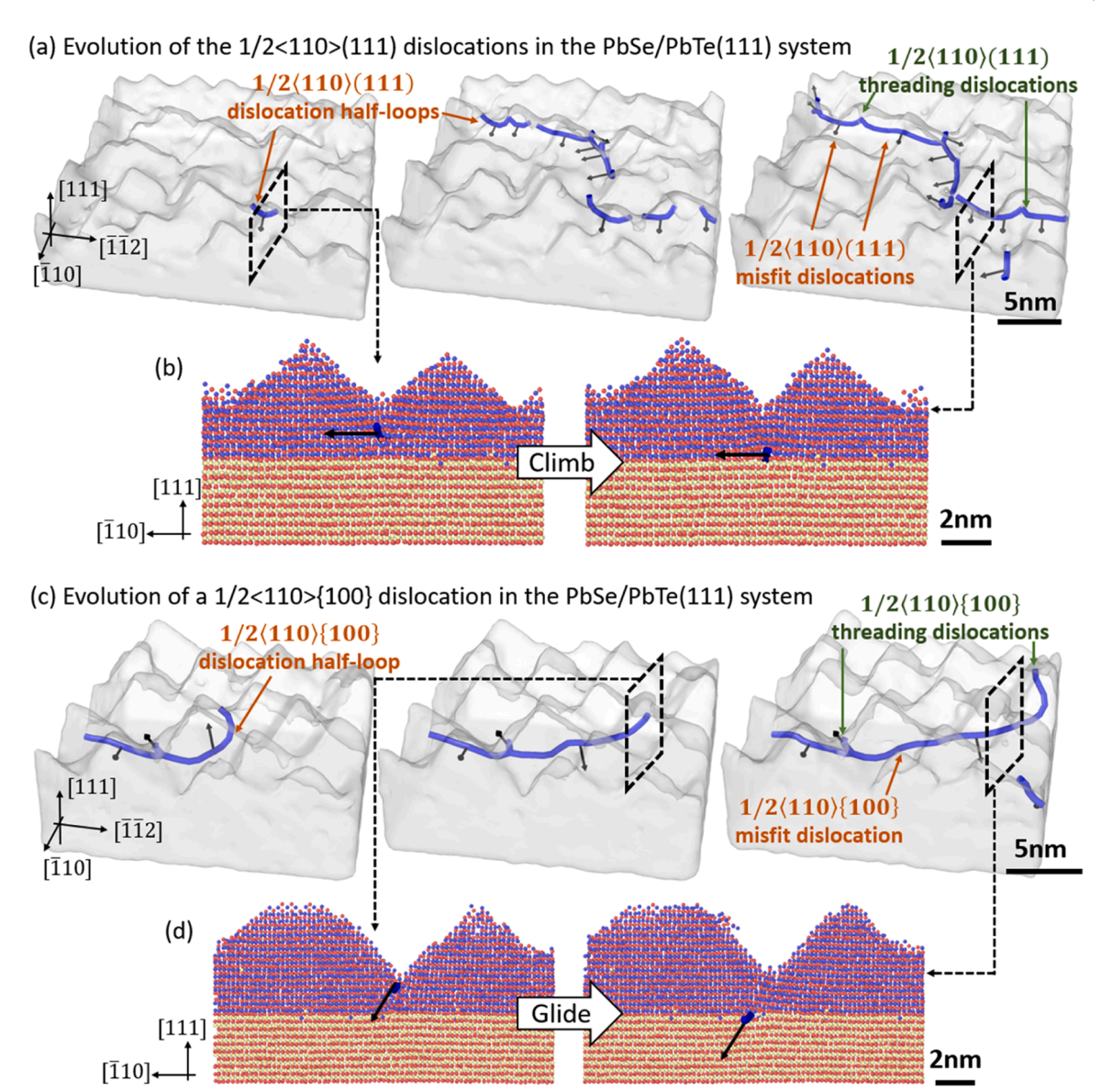


Fig. 9. (a) Evolution of the 1/2 < 110 > (111) dislocations in the PbSe/PbTe(111) heterostructure from PbSe coverage of 8.3 ML to 9.2 ML. (b) Side-views of the atomic structure in the vicinity of the dislocation in the region marked by the dashed parallelogram in (a), showing the climb migration of the 1/2 < 110 > (111) dislocation. (c) Evolution of a 1/2 < 110 > (100) dislocation in the PbSe/PbTe(111) heterostructure from PbSe coverage of 11.1 ML to 12.3 ML. (d) Side-views of the atomic structure in the vicinity of the dislocation in the region marked by the dashed parallelogram in (c), showing the glide motion of the 1/2 < 110 > (100) dislocation. Dislocations are visualized using OVITO DXA with dislocations represented by lines and Burgers vectors of dislocations represented by arrows. The epilayer surface is colored grey.

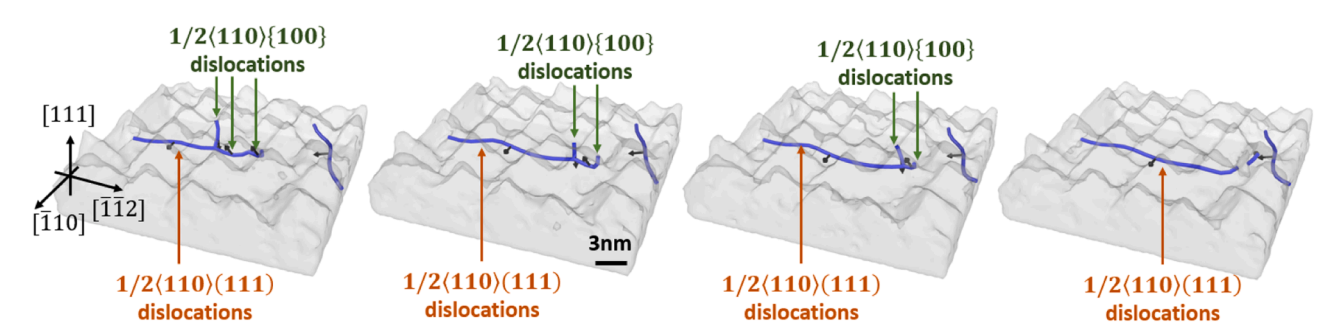


Fig. 10. Snapshots of dislocation structures in a zoom-in region of the PbSe/PbTe(111) epitaxial heterostructure, from epilayer coverage of 10.8 ML to 11 ML, showing the annihilation process of the $1/2 < 110 > \{100\}$ dislocations.

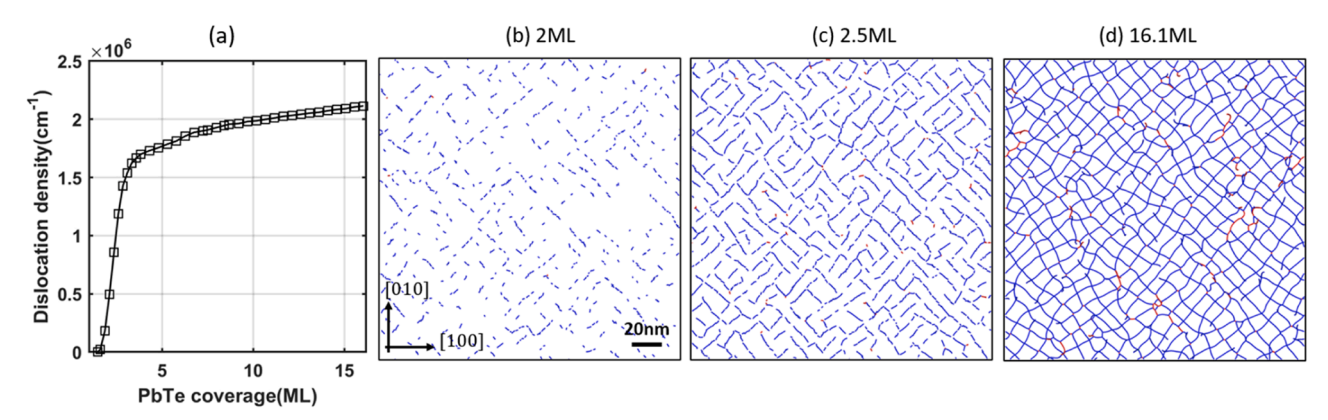


Fig. 11. (a) Dislocation density as a function of the epilayer coverage during the growth of PbTe on the PbSe(001) substrate with dimensions of $200 \times 200 \times 200 \times 200 \times 200 \times 200$ mm³. (b-d) Top views of dislocation networks in the PbTe/PbSe(001) heterostructure at different PbTe coverages. Blue and red lines denote 1/2 < 110 > (001) and 1/2 < 110 > (111) dislocations, respectively.

by dislocations. The dislocations ultimately form a relatively uniform-spaced square-like network, as shown in Fig. 11(d). The threading dislocation density at 16.1 ML PbTe coverage is calculated to be $5.11 \times 10^{11}~{\rm cm}^{-2}$.

To understand the mechanisms underlying the formation of misfit and threading dislocations in the PbTe/PbSe(001) epitaxial heterostructure, we present a time sequence of the evolution of dislocations in two zoomed-in regions of the PbTe/PbSe(001) heterostructure in Figs. 12(a) and 12(c), respectively. The atomic structures in the vicinity of the dislocations are presented in Figs. 12(b) and 12(d). Fig. 12(a) shows the evolution process of the 1/2<110>(001) dislocations over a range of PbTe coverage of 2.5 ML to 3.4 ML. Similar to the 1/2<110> (111) dislocations in the PbSe/PbTe(111) heterostructure, which have Burgers vectors parallel to the PbSe/PbTe(111) interface, the 1/2<110> (001) dislocations in the PbTe/PbSe(001) heterostructure also have Burgers vectors parallel to the PbTe/PbSe(001) interface. The evolution processes of the 1/2 < 110 > (111) dislocations and the 1/2 < 110 > (001)dislocations are similar as well; the 1/2<110>(001) dislocation halfloops nucleate from the epilayer surface, extend to the interface by vertical climb or merge with other dislocation half-loops within the same loop planes, and generate 1/2<110>(001) misfit dislocations and threading dislocations, as shown in Fig. 12(a). The climb motion of the 1/2<110>(001) dislocation can be clearly seen from Fig. 12(b). The 1/ 2<110>(001) threading dislocation segments have edge-component Burgers vectors and are of edge and/or mixed types.

Fig. 12(c) presents the evolution of $1/2 < 110 > \{111\}$ dislocations in a zoomed-in region of the PbTe/PbSe(001) structure, from PbTe coverage of 4.8 ML to 6.1 ML. The 1/2<110>{111} dislocations have the Burgers vectors inclined to the PbTe/PbSe(001) interface. They extend towards the interface through glide, as shown in Fig. 12(d). Once the $1/2 < 110 > \{111\}$ dislocations reach the interface, they form the 1/2<110>{111} misfit and threading dislocations. The simulation results show that 1/2<110>{111} misfit dislocations cannot glide along the PbTe/PbSe(001) interface, as their Burgers vectors are inclined to the interface. Consequently, once formed, the 1/2<110>{111} misfit dislocations are stationary at the interface and can only extend or annihilate. Therefore, the spatial distribution of the 1/2<110>{111} misfit dislocations is random, interspersed in the square-like network of the 1/ 2<110>(001) misfit dislocations, as shown in Fig. 11(d). The 1/ 2<110>{111} threading dislocation segments have screw-component Burgers vectors and are of screw and/or mixed types.

Simulation results show that 1/2<110>{111} dislocations can annihilate during the growth of PbTe on PbSe(001). Fig. 13 presents an annihilation process of two 1/2<110>{111} dislocation segments in the PbTe/PbSe(001) structure. The Burgers vectors of the two 1/2<110>{111} dislocation segments are a/2[011] and $a/2[\overline{1}0\overline{1}]$. As can be seen in Fig. 13, the 1/2<110>{111} dislocation segments form a dislocation

loop and then transit to a dislocation junction. During the process, the 1/2 < 110 > (001) dislocation with Burgers vector of $a/2[\overline{1}10]$ that is connected to the two $1/2 < 110 > \{111\}$ dislocations elongates, indicating that the two $1/2 < 110 > \{111\}$ dislocations annihilate and generate the 1/2 < 110 > (001) dislocation segment. The process can be described by the reaction: $a/2[011] + a/2[\overline{1}0\overline{1}] \rightarrow a/2[\overline{1}10]$. Similar to the annihilation processes of $1/2 < 110 > \{100\}$ dislocations in the PbSe/PbTe(111) system, the annihilation processes of $1/2 < 110 > \{110\}$ dislocations in the PbTe/PbSe(001) system reduce the system potential energy and hence are energetically favorable as well.

In summary, during the growth of the two PbTe/PbSe epitaxial heterostructures, dislocations are first nucleated from the epilayer surface and then extend to the interface and form misfit and threading dislocations. The characteristics of the dislocations that are generated during these processes are summarized in Table 1. As discussed previously, dislocations with Burgers vectors parallel to the interface are the dominant type in both systems. These dislocations extend to the interface through climb and merge with other dislocations, generating edgetype misfit and edge-type or mixed-type threading dislocations. Conversely, dislocations with Burgers vectors inclined to the interface are a minor type in both systems. They propagate to the interface through glide and form edge-type misfit dislocations and screw-type or mixed-type threading dislocations.

The critical thickness for dislocation nucleation in the PbSe/PbTe (111) structure is found to be 7.5 ML, while that of the PbTe/PbSe(001) structure is 1.4 ML. The relatively larger critical thickness for dislocation nucleation in the PbSe/PbTe(111) structure compared to the PbTe/PbSe (001) structure can be explained by two factors. First, the growth of PbSe on the PbTe(111) substrate follows the SK growth mode. This leads to the growth of PbSe islands, which relieves the mismatch strain at the initial stage of growth, thereby suppressing the nucleation of dislocations. In contrast, the growth of PbTe on the PbSe(001) substrate follows the layer-by-layer growth mode. As a result, all the mismatch strain needs to be relieved by dislocation formation. Second, the dominant dislocations in the PbSe/PbTe(111) structure are 1/2<110>(111) dislocations, while the dominant dislocations in the PbTe/PbSe(001) structure are 1/2 < 110 > (001) dislocations. It is noted that $< 110 > \{100\}$ slip systems are the primary slip systems of lead salts[71,72]. In the Appendix, we have computed the Peierls stresses of 1/2<110>{111} and 1/2<110>{100} edge dislocations in PbTe and PbSe single crystals, respectively, as well as of misfit dislocations in the PbTe/PbSe heterosystems, as shown in Table A1. It shows that the Peierls stress of the 1/2<110>{111} dislocation in PbSe is about 9 times that of the 1/2<110>{100} dislocation in PbTe, indicating that the nucleation of 1/2<110>(111) dislocations in the PbSe epilayer on the PbTe(111) substrate is more difficult compared to the nucleation of 1/2<110> (001) dislocations in the PbTe epilayer on the PbSe(001) substrate.

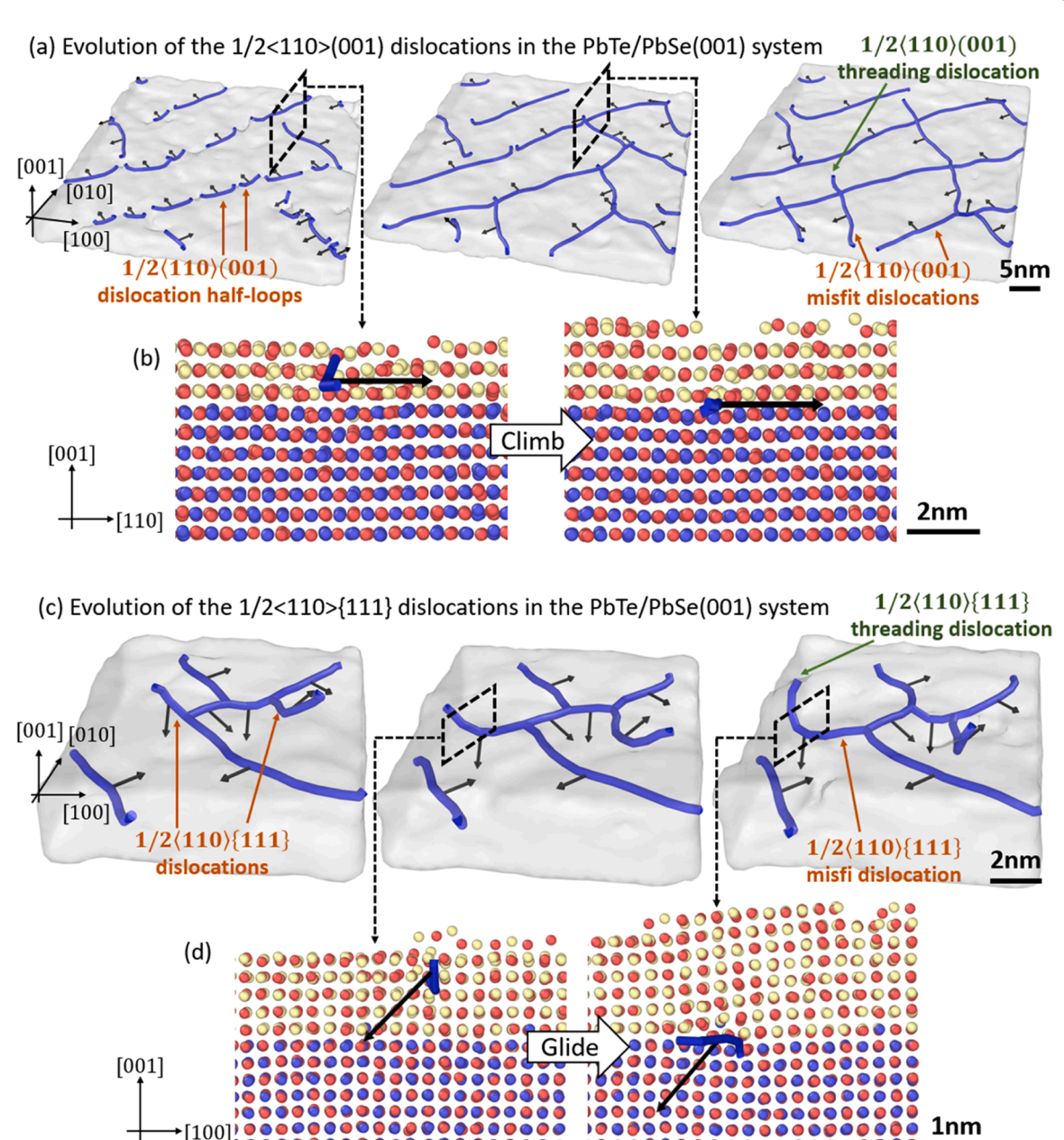


Fig. 12. (a) Evolution of the 1/2 < 110 > (001) dislocations in the PbTe/PbSe(001) heterostructure from PbTe coverage of 2.5 ML to 3.4 ML. (b) Side-views of the atomic structure in the vicinity of the dislocation in the region marked by the dashed parallelogram in (a), showing the climb migration of the 1/2 < 110 > (001) dislocation. (c) Evolution of the 1/2 < 110 > (111) dislocations in the PbTe/PbSe(001) heterostructure from PbTe coverage of 4.8 ML to 6.1 ML. (d) Side-views of the atomic structure in the vicinity of the dislocation in the region marked by the dashed parallelogram in (c), showing the glide motion of the 1/2 < 110 > (111) dislocation.

As can be seen from Figs. 5(a) and 6(a), the hexagonal-like 1/2 < 110 > (111) misfit dislocation network in the PbSe/PbTe(111) heterostructure has less uniformity compared to the square-like 1/2 < 110 > (001) misfit dislocation network in the PbTe/PbSe(001) heterostructure. One reason for this difference is that although both types of misfit dislocations tend to form networks with uniform spacing under the mutual repulsive interaction between neighboring misfit dislocations, the glide of 1/2 < 110 > (111) misfit dislocations within the PbSe/PbTe(111) interface is more difficult than the glide of 1/2 < 110 > (001) misfit dislocations within the PbTe/PbSe(001) interface due to the approximately 20% higher Peierls stress, as shown in Table 1. The high mobility of 1/2 < 110 > (001) dislocations within the PbTe/PbSe(001) interface can be evidently observed in Fig. 12(a), where some 1/2 < 110 > (001) dislocations have moved away from their initial positions of nucleation.

Another possible reason is that the growth of PbSe on the PbTe(111) substrate is accompanied by significant elastic substrate deformation, which is non-uniformly distributed and results in a non-uniformly distributed misfit dislocation network. This is demonstrated to be the main reason for the low uniformity of the hexagonal-like 1/2 < 110 > (111) misfit dislocation network in the PbSe/PbTe(111) heterostructure and will be discussed more in Section 3.4.

3.4. Effect of substrate size

The effect of "substrate deformation" has been repeatedly investigated in experimental studies of heteroepitaxial growth[21,22,73]. One such demonstration is the experiment of Eaglesham and Cerullo who showed that "dislocation-free islands of pure Ge can be grown on Si

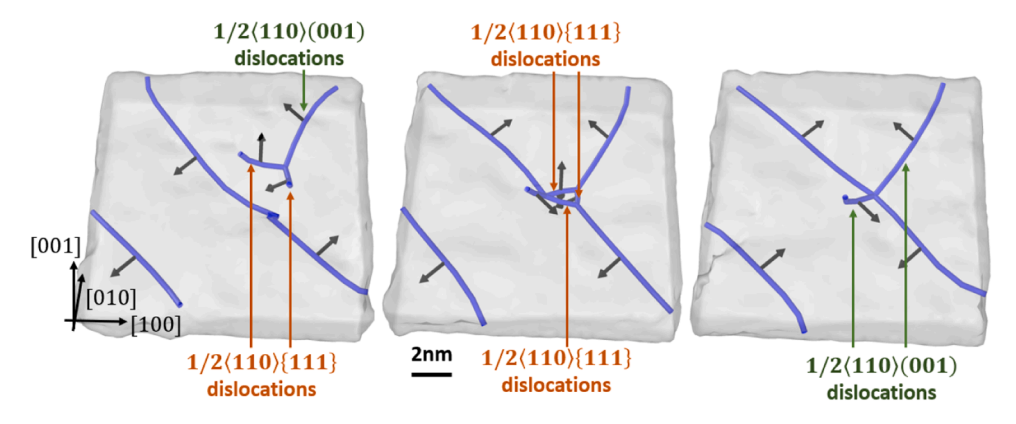


Fig. 13. Snapshots of dislocation structures in a zoom-in region of the PbTe/PbSe(001) epitaxial heterostructure, from epilayer coverage of 3.5 ML to 4.3 ML, showing the annihilation process of the $1/2 < 110 > \{111\}$ dislocations.

Table 1
Characteristics of dislocations generated during the growth processes of the PbSe/PbTe(111) and PbTe/PbSe(001) epitaxial heterostructures.

| Heterostructure | Dislocations nucleated from free surface | Burgers vector | Extension behavior | Misfit and threading dislocations | Length distribution |
|--------------------|--|---------------------------|--------------------|---|---------------------|
| PbSe/PbTe | 1/2<110>(111) | Parallel to the interface | Climb | 1/2<110>(111) misfit dislocation (Edge) | 90.3% |
| (111) | | | & | & | |
| | | | merge | 1/2<110>(111) threading dislocations | |
| | | | | (Edge or mixed) | |
| | 1/2<110>{100} | Inclined to the interface | Glide | 1/2<110>{100} misfit dislocation (Edge) | 9.7% |
| | | | | & | |
| | | | | 1/2<110>{100} threading dislocations | |
| | | | | (Screw or mixed) | |
| PbTe/PbSe (001) | 1/2<110>(001) | Parallel to the interface | Climb | 1/2<110>(001) misfit dislocation (Edge) | 94.7% |
| | | | & | & | |
| | | | merge | 1/2<110>(001) threading dislocations | |
| | | | | (Edge or mixed) | |
| | 1/2<110>{111} | Inclined to the interface | Glide | 1/2<110>{111} misfit dislocation (Edge) | 5.3% |
| | | | | & | |
| | | | | 1/2<110>{111} threading dislocations | |
| | | | | (Screw or mixed) | |

(100) up to 0.14 µm diameter and 500 Å thickness" [73], and that the nearly 2 orders of magnitude increase in the critical thickness, compared to the usual $\sim\!1$ nm critical thickness for Ge thin films on Si substrate, was attributed to the "local substrate deformation" [73]. To quantify the mesoscopic effects of the substrate on growth, we have performed a series of CAC simulations with substrates of four different dimensions: $50\!\times\!50\!\times\!10$ nm³, $100\!\times\!100\!\times\!10$ nm³, $100\!\times\!100\!\times\!100$ nm³, and $200\!\times\!200\!\times\!200$ nm³. It is noted that a 10 nm-thick substrate with the

bottom layer fixed has never been used in real epitaxial growth. It is included in this comparison because it is the typical substrate size and boundary conditions that have been used in existing MD simulations for heteroepitaxial growth[20,65].

In Fig. 14, we present the dislocation density in the PbSe/PbTe(111) and PbTe/PbSe(001) epitaxial heterostructure as a function of the epilayer coverage and substrate size. It is seen from Fig. 14(a) that the dislocation density in the PbSe/PbTe(111) structure is very sensitive to

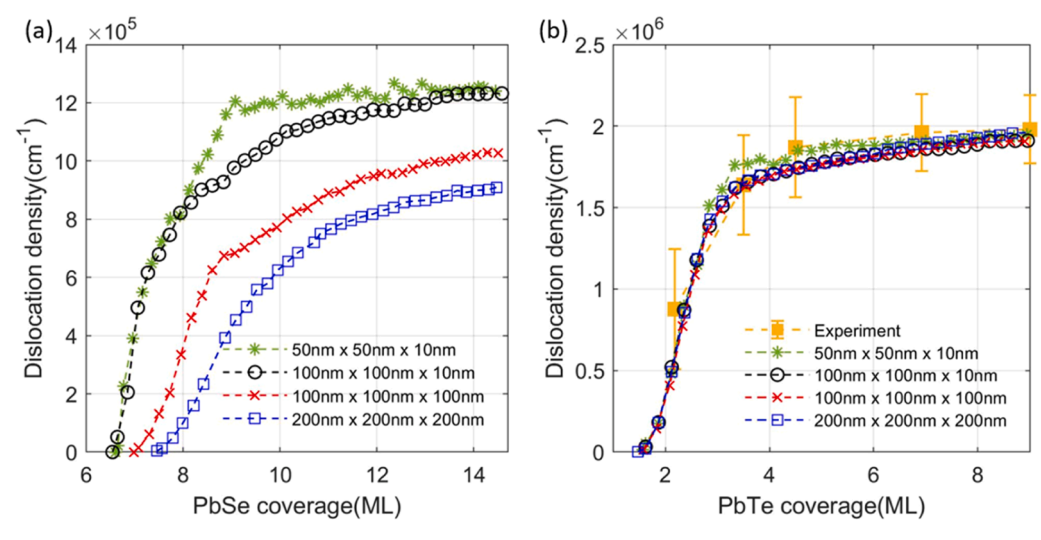


Fig. 14. Dislocation density in the PbSe/PbTe(111) and PbTe/PbSe(001) heteroepitaxial structures, as a function of the epilayer coverage and substrate size.

the size of the substrate. The critical thickness for dislocation nucleation increases from 6.6 ML to 7.5 ML as the substrate size increases from $50\times50\times10~\text{nm}^3$ to $200\times200\times200~\text{mm}^3$. Additionally, the dislocation density is shown to decrease with increasing substrate size. For example, the dislocation density at an epilayer coverage of 14 ML is $1.26\times10^6~\text{cm}^{-1}$ for the $50\times50\times10~\text{nm}^3$ substrate, which is 40% higher than the dislocation density of $9\times10^5~\text{cm}^{-1}$ for the $200\times200\times200~\text{mm}[3]$ substrate at the same coverage. These results suggest that a larger substrate shares more strain energy of a strained heterostructure, leading to a significantly reduced dislocation density.

In contrast, the effect of substrate size on dislocation formation in the PbTe/PbSe(001) system is found to be negligible. It is seen from Fig. 14 (b) that the evolution of dislocation density in the PbTe/PbSe(001) structures with differently sized substrates are similar, and are very close to the experimental results[61], indicating that the substrate size does not have a significant effect on the formation and evolution of dislocations in the system. This is because the growth of PbTe on PbSe(001) follows the layer-by-layer growth mode and dislocations start to nucleate at the very beginning of the growth process, which effectively relieves the lattice mismatch strain in the system. As a result, the mismatch strain does not cause the substrate to significantly deform. Thus, the effect of the substrate size on the nucleation and evolution of dislocations in the PbTe/PbSe(001) system is limited.

Fig. 15 compares the dislocation networks in PbSe grown on the PbTe(111) substrates of different sizes. It is evident that the dislocation network in the system with a $100 \times 100 \times 10$ nm³ substrate is more regular than that in the system with a $200 \times 200 \times 200$ nm³ substrate. In the former, the spacing of the dislocation network ranges from 14 nm to 20 nm. However, in the latter, the spacing varies widely from 10 nm to 45 nm. This difference is due to the different deformations of substrates that relieve the lattice mismatch strain in the epilayers. Our simulation results show that the deformation is less uniformly distributed in larger substrates than that in smaller substrates. As a result, the spatial distribution of the dislocations in larger substrates is less regular. This explains the less uniformity of the hexagonal-like misfit dislocation network in the PbSe/PbTe(111) system compared to the square-like misfit dislocation network in the PbTe/PbSe(001) system, as the substrate deformation in the former is much more significant than the latter. Furthermore, as the size of the PbTe(111) substrate increases, the percentage of 1/2<110>{100} dislocations among all dislocations in the PbSe/PbTe(111) system increases. This can be attributed to the higher shear distortion capacity of larger substrates along the direction inclined to the interface, resulting in the activation of more 1/2<110>{100} dislocations with Burgers vectors inclined to the interface.

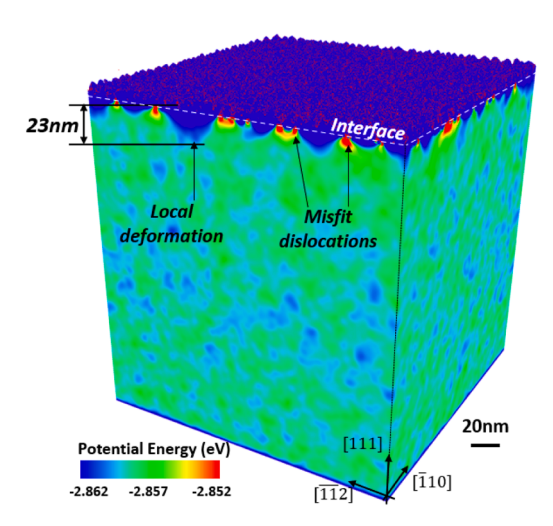


Fig. 16. Potential energy of the PbSe/PbTe(111) epitaxial heterostructure with a $200\times200\times200$ nm³ substrate.

In Fig. 16 we present the potential energy distribution of the PbSe/PbTe(111) epitaxial heterostructure containing a $200\times200\times200$ nm³ substrate. The high-energy regions at the interface stem from the misfit dislocations. Coherent interface regions can be observed between misfit dislocations. It can be seen from Fig. 16 that the potential energy of the substrate regions near the coherent interface regions is significantly different from those of regions away from the interface, indicating that the substrate regions beneath the coherent interface are experiencing local deformation. This local substrate deformation is observable even at a depth greater than 20 nm below the interface. In addition, it is evident that the substrate deformation is non-uniformly distributed along the interface. These results provide direct evidence of significant substrate deformation in the PbSe/PbTe(111) heteroepitaxial structure.

4. Summary and discussion

In this study, we have simulated the kinetic processes of the epitaxial growth of PbSe/PbTe(111) and PbTe/PbSe(001) systems using the CAC method as the simulation tool. A comparison between CAC and MD simulation results has been conducted to test the accuracy of CAC in reproducing the results of fully atomistic resolved simulations. We have observed the SK growth mode during the growth of PbSe on PbTe(111) and the layer-by-layer growth mode during the growth of PbTe on PbSe

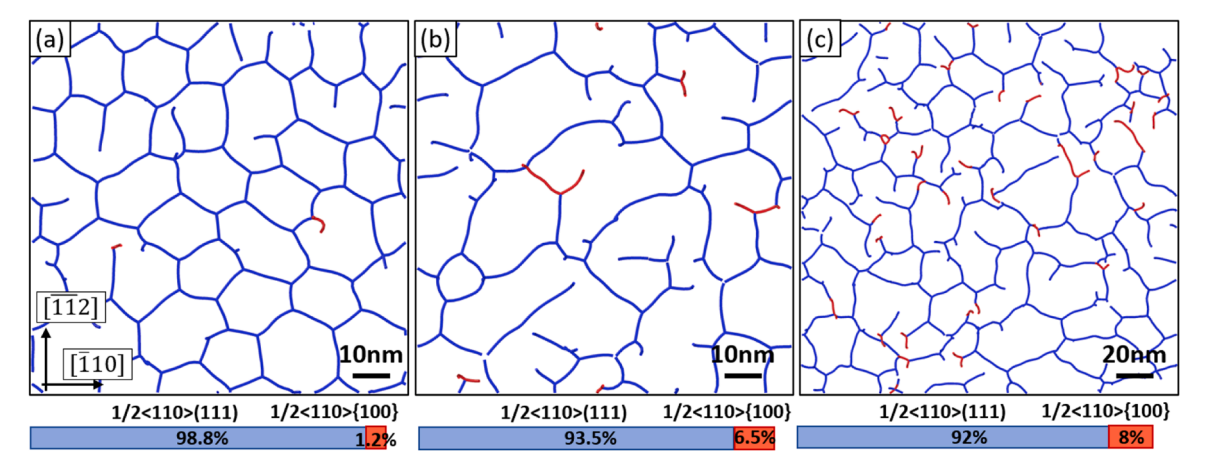


Fig. 15. Top views of dislocation networks in the growth simulations of the PbSe/PbTe(111) heteroepitaxial structures at 14 ML epilayer coverage with substrates of different dimensions: (a) $100 \times 100 \times 100 \times 10$ nm³, (b) $100 \times 100 \times 100 \times 100$ nm³, and (c) $200 \times 200 \times 200$ nm³. Blue and red lines denote the 1/2 < 110 > (111) and 1/2 < 110 > (100) dislocations, respectively. The percentage of 1/2 < 110 > (111) and 1/2 < 110 > (100) dislocations based on the calculation of dislocation lengths are shown at the bottom of each figure.

(001). We have also observed the formation of pyramid-shaped PbSe islands in the PbSe/PbTe(111) system and square-like misfit dislocation networks in the PbTe/PbSe(001) system. These results agree very well with the experimental observations[61-63], including the evolution of dislocation density with epilayer thickness (Fig. 14b). Furthermore, we have captured the hexagonal-like misfit dislocation network in the PbSe/PbTe(111) structure and provided clear visualizations of the atomic structures of the four types of misfit dislocations in the PbSe/PbTe(111) and PbTe/PbSe(001) heteroepitaxial structures. These results demonstrate the efficacy of the CAC method in addressing the length-scale challenge for simulations of heteroepitaxy without any empirical assumptions about defect type, defect structure, and formation mechanisms. We have shown that a predictive mesoscopic simulation method such as CAC is necessary to understand size scale effects on the growth process and accommodation of misfit strain in certain systems; in this case, it was demonstrated that the growth of PbSe/PbTe (111) heteroepitaxial structures is highly sensitive to the size of the model, differing substantially in terms of accommodational interface dislocation densities and structure. The results remain scale-sensitive even for the largest substrate $(200\times200\times200 \text{ nm}^3)$, suggesting the need to pursue even larger scale simulations which are intractable via MD. Application of CAC illuminates the mechanisms which engender this scale dependence and lead to different self-organized dislocation structures as a function of substrate size; hence, certain heteroepitaxy processes demand multiscale simulations while for others, MD will suffice.

There are several key findings regarding the formation of misfit dislocations in PbSe/PbTe heterosystems.

- (1) The formation process of misfit dislocations can be divided into three main steps:
 - a) Dislocation half-loops nucleate from the free surfaces of the epilayer. Specifically, the 1/2 < 110 > (111) and $1/2 < 110 > \{100\}$ dislocation half-loops are formed in the PbSe/PbTe (111) system; the 1/2 < 110 > (001) and $1/2 < 110 > \{111\}$ dislocation half-loops are formed in the PbTe/PbSe(001) system.
 - b) The dislocation half-loops with Burgers vectors parallel to the interface extend towards the interface via climb and merge with other half-loops in the same plane, whereas the dislocation half-loops with Burgers vectors inclined to the interface extend towards the interface via glide.
 - c) Once the dislocation half-loops reach the interface, they form misfit dislocations and threading dislocations on the same slip systems as the dislocation half-loops.
- (2) The dominant dislocation types in both systems are those with Burgers vectors parallel to the interface, i.e., 1/2<110>(111) misfit dislocations in the PbSe/PbTe(111) system and 1/2<110> (001) misfit dislocations in the PbTe/PbSe(001) system. These dislocations are most effective at relieving the lattice mismatch strain and minimizing the system's potential energy.

- (3) The dislocations with Burgers vectors inclined to the interface have the tendency to annihilate during the growth processes, including the 1/2<110>{100} dislocations in the PbSe/PbTe (111) system and the 1/2<110>{111} dislocations in the PbTe/PbSe(001) system. The annihilation processes are accompanied by the generation of new dislocations with Burgers vectors parallel to the interface. These annihilation processes are energetically favorable and reduce the system's energy.
- (4) The substrate size and deformation have a significant effect on the dislocation formation and evolution during the growth of PbSe on PbTe(111). Larger substrates undergo larger deformation during growth, leading to more relief of the lattice mismatch strain, higher critical thickness for dislocation nucleation, and lower dislocation density. Larger substrates also result in nonuniform spatial distributions of misfit dislocations and increase the likelihood of the generation of dislocations with Burgers vectors inclined to the interface. These results provide insight into the effect of substrate size and deformation on dislocation formation and evolution in heteroepitaxy. They also provide a quantitative understanding of the importance of accurately simulating the substrate dimensions used in experiments to ensure reliable simulation results.

Finally we would like to note that this work focuses on epitaxial growth on defect-free substrates, as defect-free substrates are desirable for heteroepitaxy and the technology to fabricate nearly defect-free PbTe and PbSe substrates has been achieved[71,74]. Nevertheless, it is straightforward for the CAC method to simulate substrates with dislocations. The rhombohedral-shaped FEs employed in modeling the substrates enable the nucleation and glide of dislocations in the substrates between elements on either of (100) or (111) slip systems along the element boundaries. Investigation of the effect of defects in the substrates on heteroepitaxy is one of our on-going research endeavors.

Declaration of Competing Interest

The authors declare that they have no known competing financial interests or personal relationships that could have appeared to influence the work reported in this paper.

Acknowledgement

This work is based on research supported by the US National Science Foundation under Award Number CMMI-2054607. The work of Chen and Phillpot is also partially supported by DMR 2121895. The computer simulations are funded by the Advanced Cyberinfrastructure Coordination Ecosystem: Services & Support (ACCESS) allocation TG-DMR190008. McDowell is grateful for the support of the Carter N. Paden, Jr. Distinguished Chair in Metals Processing at Georgia Tech.

Appendix. A. Peierls stresses in PbTe and PbSe single crystals, and at PbTe/PbSe interfaces

The method proposed by Osetsky and Bacon[75] is adopted in this work to compute the Peierls stresses of $1/2 < 110 > \{111\}$ and $1/2 < 110 > \{100\}$ edge dislocations in PbTe and PbSe single crystals, respectively, as well as the Peierls stresses of misfit dislocations within the PbTe/PbSe heterointerfaces. There are effectively three steps for determining the Peierls stress:

(1) Creation of a model containing an edge dislocation: An initial model consisting of two PbSe (or PbTe) half-crystals in contact at the (100) or (111) surface is constructed, as shown in Fig. A1(a). The upper half-crystal possesses one additional lattice plane perpendicular to the Y direction compared to the lower half-crystal. For instance, the upper and lower half-crystals comprise N and (N-1) lattice planes, respectively. The repeat distance of the lattice planes in the upper and lower half-crystals along the Y direction is, respectively, 1/2N smaller and larger than that of the perfect crystal. This ensures that the dimensions of the upper and lower half-crystals along the Y direction are similar. In this work, N=100 and N=200 are studied, respectively. The dimensions of the model along the X and Z directions are 5 nm and 50 nm, respectively.

Periodic boundary conditions (PBC) are applied along the X and Y directions. The model is relaxed at 650K for 100 ps and then cooled down to a temperature close to 0 K. After relaxation, an edge dislocation along the X direction with the Burgers vector along the Y direction is formed in the center of the model. Using this method, we obtain the edge dislocations in PbSe (or PbTe) single crystal. The atomic structures of $1/2 < 110 > \{111\}$ and $1/2 < 110 > \{100\}$ edge dislocations in PbSe are shown in Figs. A1(b) and A1(c), respectively. The atomic structures of the edge dislocations in PbTe are similar.

- (2) Creation of a model containing a misfit dislocation: An initial PbTe/PbSe bicrystal model is constructed, containing PbTe and PbSe single crystals in contact at the (001) or (111) surface. At the interface, which lies in the X-Y plane, there are 4×18 PbTe unit cells and 4×19 PbSe unit cells. The numbers of unit cells along the Y direction are determined according to the lattice mismatch between PbTe and PbSe and the concept of coincidence site lattice on the misfit interface[76], which allows the relaxation of the stress induced by the lattice mismatch at the interface. The numbers of unit cells along the X direction are set to be small to prevent misfit dislocations with Burgers vectors along the X direction from nucleating. The dimension of the model along the Z direction is 50 nm. PBCs are applied along the X and Y directions. A simulation that mimics the direct wafer bonding process is performed, creating a misfit dislocation with the dislocation line along the X direction and the Burgers vector along the Y direction at the center of the model. Details of simulations of the direct wafer bonding process can be seen in ref.[50]. Using this method, we obtain the misfit dislocations at the PbTe/PbSe interfaces. The atomic structures of a 1/2<110>(111) misfit dislocation within the PbSe/PbTe(111) interface and a 1/2<110>(001) misfit dislocation within the PbTe/PbSe(001) interface are shown in Fig. A1(d) and A1(e), respectively.
- (3) Apply a shear force to the model: An external force, F, is exerted on the top atomic layer of the model along the direction of the Burgers vectors of the dislocations (i.e., Y direction), as shown in Fig. A2. The applied force F can be incremented over time according to the designated rate. The top atomic layer of the model can move along the X and Y directions in response to the external force, while the bottom atomic layer is fixed, and the rest of the atoms are free to move. PBCs are applied along the X and Y directions. The applied force creates shear stress in the model, which can be calculated as $\sigma_{Xy} = F/A_{Xy}$, where A_{Xy} is the X-Y cross-sectional area of the model. We incrementally increase F and perform full atomic relaxation after each increment. Initially, the model undergoes elastic deformation. Once a critical stress is reached, the dislocation core moves, and the crystal undergoes plastic deformation. The critical stress corresponds to the Peierls stress of the dislocation.

Using the aforementioned method, we have computed the Peierls stresses of dislocations in PbTe and PbSe single crystals, respectively, and of misfit dislocations at the PbTe/PbSe interfaces. The results are shown in Table A1. To quantify the size effect of the simulation box on Peierls stress, we have doubled the simulation cell size of the single crystal models along the Y and Z directions and the simulation cell size of the PbTe/PbSe models along the Z direction. Simulation results show that the effect of simulation cell size on the Peierls stress is negligible over the size range investigated. This indicates that the cell size we used is adequate for determination of the Peierls stress. Our results show that the Peierls stress of the 1/2 < 110 > 100 edge dislocation is lower than that of the 1/2 < 110 > 111 edge dislocation in both PbTe and PbSe single crystals, which is consistent with the experimental observations that 10 > 100 are the primary slip systems of lead salts[71,72].

Table A1Peierls stresses computed in simulations.

| Dislocation | Peierls stress (MPa) | |
|---|----------------------|--|
| <110>{100} dislocation in PbTe | 1.15 | |
| <110>{111} dislocation in PbTe | 1.23 | |
| <110>{100} dislocation in PbSe | 5.74 | |
| <110>{111} dislocation in PbSe | 10.65 | |
| <100>{100} misfit dislocation within the PbTe/PbTe(001) interface | 1.98 | |
| <100>{111} misfit dislocation within the PbSe/PbTe(111) interface | 2.41 | |

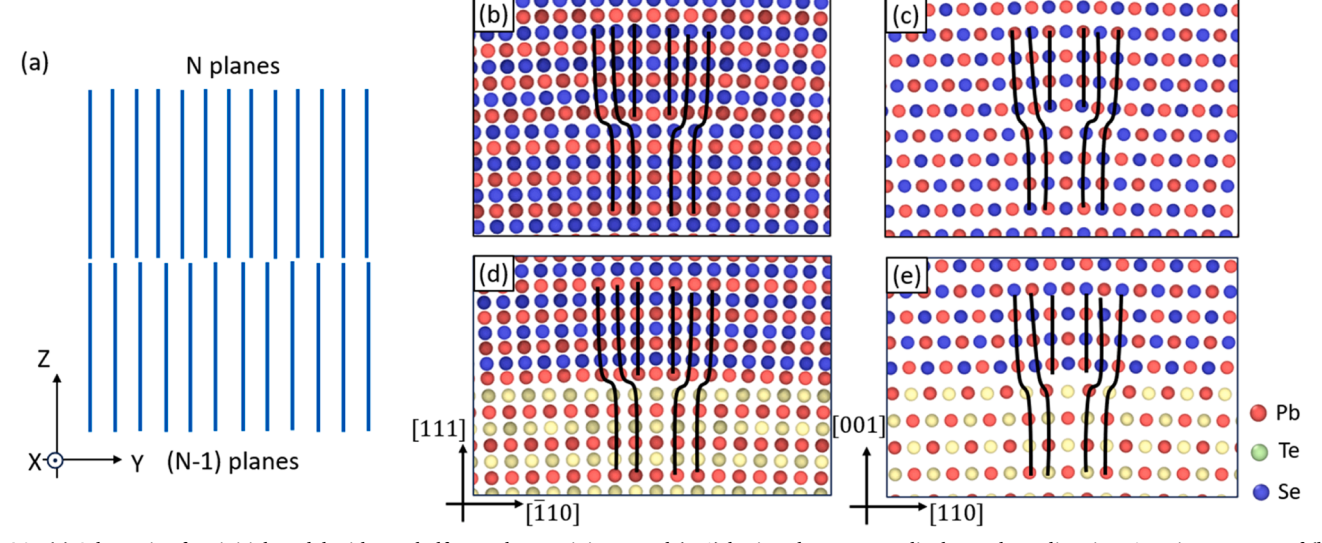


Fig. A1. (a) Schematic of an initial model with two half-crystals containing N and (N-1) lattice planes perpendicular to the Y direction. Atomic structures of (b)1/2<110>{111} and (c)1/2<110>{100} edge dislocations in the PbSe single crystals, and the (d)1/2<110>(111) misfit dislocations within the PbSe/PbTe(111) interface and (e)1/2<110>(001) misfit dislocations within the PbTe/PbSe(001) interface.

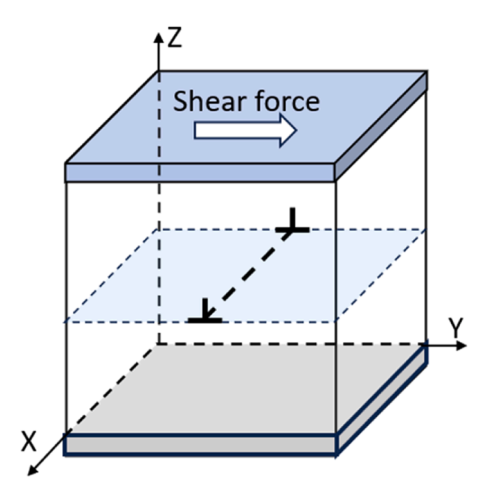


Fig. A2. Simulation configuration used to compute the Peierls stress of an edge dislocation or a misfit dislocation. The dislocation is generated in the center of the simulation box and can belong to a {111} or a {100} slip plane.

References

- Y.-Y. Wong, et al., The roles of threading dislocations on electrical properties of AlGaN/GaN heterostructure grown by MBE, J. Electrochem. Soc. 157 (2010) H746–H749.
- [2] Z. Bougrioua, et al., Engineering of an insulating buffer and use of AlN interlayers: two optimisations for AlGaN–GaN HEMT-like structures, Physica Status Solidi (a) 195 (2003) 93–100.
- [3] Murray, C. Department of Energy Basic Research Needs for Microelectronics, Report of the Office of Science Workshop on Basic Research Needs for Microelectronics (2018).
- [4] F.C. Frank, J. Van der Merwe, One-dimensional dislocations. II. Misfitting monolayers and oriented overgrowth, Proc. R. Soc. Lond. A 198 (1949) 216–225.
- [5] F. Frank, J.H. van der Merwe, One-dimensional dislocations. I. Static theory, Proc. R. Soc. Lond. A 198 (1949) 205–216.
- [6] J.H. Van Der Merwe, Crystal interfaces. part II. finite overgrowths, J. Appl. Phys. 34 (1963) 123–127.
- [7] Stowell, M. & Matthews, J. (Academic Press New York, 1975).
- [8] J. Matthews, A. Blakeslee, Defects in epitaxial multilayers: I. Misfit dislocations, J. Cryst. Growth 27 (1974) 118–125.
- [9] J.W. Matthews, A.E. Blakeslee, Defects in epitaxial multilayers, J. Cryst. Growth 27 (1974) 118–125, https://doi.org/10.1016/S0022-0248(74)80055-2.
- [10] A. Romanov, W. Pompe, G. Beltz, J. Speck, Modeling of Threading Dislocation density reduction in heteroepitaxial layers, Phys. Stat. Sol. (b) 198 (1996) 599.
- [11] D.J. Eaglesham, M. Cerullo, Dislocation-free stranski-krastanow growth of Ge on Si (100), Phys. Rev. Lett. 64 (1990) 1943.
- [12] J. Narayan, S. Sharan, Mechanism of formation of 60 and 90 misfit dislocations in semiconductor heterostructures, Mater. Sci. Eng.: B 10 (1991) 261–267.
- [13] E. Kasper, H.J. Herzog, H. Kibbel, A one-dimensional SiGe superlattice grown by UHV epitaxy, Appl. Phys. 8 (1975) 199–205, https://doi.org/10.1007/ BF00896611.
- [14] R. People, J. Bean, Calculation of critical layer thickness versus lattice mismatch for Ge x Si1- x/Si strained-layer heterostructures, Appl. Phys. Lett. 47 (1985) 322-324.
- [15] L. Dong, J. Schnitker, R.W. Smith, D.J. Srolovitz, Stress relaxation and misfit dislocation nucleation in the growth of misfitting films: A molecular dynamics simulation study, J. Appl. Phys. 83 (1998) 217–227.
- [16] F. Much, M. Ahr, M. Biehl, W. Kinzel, A kinetic Monte Carlo method for the simulation of heteroepitaxial growth, Comput. Phys. Commun. 147 (2002) 226–229.
- [17] S.M. Wise, J.S. Lowengrub, J.S. Kim, W.C. Johnson, Efficient phase-field simulation of quantum dot formation in a strained heteroepitaxial film, Superlattices Microstruct. 36 (2004) 293–304.
- [18] N. Zhou, L. Zhou, A fusion-crystalization mechanism for nucleation of misfit dislocations in FCC epitaxial films, J. Cryst. Growth 289 (2006) 681–685.
- [19] J.J. Chavez, X.W. Zhou, S.F. Almeida, R. Aguirre, D. Zubia, Molecular Dynamics Simulations of CdTe/CdS Heteroepitaxy-Effect of Substrate Orientation, J. Mater. Sci. Res 5 (2016) 1.
- [20] J. Gruber, X.W. Zhou, R.E. Jones, S.R. Lee, G.J. Tucker, Molecular dynamics studies of defect formation during heteroepitaxial growth of InGaN alloys on (0001) GaN surfaces, J. Appl. Phys. 121 (2017), 195301.
- [21] C.W. Snyder, B.G. Orr, D. Kessler, L.M. Sander, Effect of strain on surface morphology in highly strained InGaAs films, Phys. Rev. Lett. 66 (1991) 3032.
- [22] S. Guha, A. Madhukar, K.C. Rajkumar, Onset of incoherency and defect introduction in the initial stages of molecular beam epitaxical growth of highly strained In x Ga1- x As on GaAs (100), Appl. Phys. Lett. 57 (1990) 2110–2112.
- [23] Y. Chen, S. Shabanov, D.L. McDowell, Concurrent atomistic-continuum modeling of crystalline materials, J. Appl. Phys. 126 (2019), 101101.

- [24] Y. Chen, Reformulation of microscopic balance equations for multiscale materials modeling, J. Chem. Phys. 130 (2009), 134706.
- [25] Y. Chen, J. Lee, Atomistic formulation of a multiscale field theory for nano/micro solids, Philos. Mag. 85 (2005) 4095–4126.
- [26] J. Irving, J.G. Kirkwood, The statistical mechanical theory of transport processes. IV. The equations of hydrodynamics, J. Chem. Phys. 18 (1950) 817–829.
- [27] Y. Chen, A. Diaz, Physical foundation and consistent formulation of atomic-level fluxes in transport processes, Phys. Rev. E 98 (2018), 052113.
- [28] Y. Chen, A. Diaz, Local momentum and heat fluxes in transient transport processes and inhomogeneous systems, Phys. Rev. E 94 (2016), 053309.
- and inhomogeneous systems, Phys. Rev. E 94 (2016), 053309.
 [29] Y. Chen, The origin of the distinction between microscopic formulas for stress and Cauchy stress, EPL 116 (2016) 34003.
- [30] Q. Deng, L. Xiong, Y. Chen, Coarse-graining atomistic dynamics of brittle fracture by finite element method, Int. J. Plast. 26 (2010) 1402–1414.
- [31] Q. Deng, Y. Chen, A coarse-grained atomistic method for 3D dynamic fracture simulation, J. Multiscale Computat. Eng. 11 (2013) 227–237.
- [32] L. Xiong, Y. Chen, Coarse-grained simulations of single-crystal silicon, Modelling Simul. Mater. Sci. Eng. 17 (2009), 035002.
- [33] L. Xiong, Q. Deng, G. Tucker, D.L. McDowell, Y. Chen, A concurrent scheme for passing dislocations from atomistic to continuum domains, Acta Mater. 60 (2012) 899–913.
- [34] L. Xiong, G. Tucker, D.L. McDowell, Y. Chen, Coarse-grained atomistic simulation of dislocations, J. Mech. Phys. Solids 59 (2011) 160–177.
- [35] S. Yang, L. Xiong, Q. Deng, Y. Chen, Concurrent atomistic and continuum simulation of strontium titanate, Acta Mater. 61 (2013) 89–102.
- [36] L. Xiong, et al., Coarse-grained elastodynamics of fast moving dislocations, Acta Mater. 104 (2016) 143–155.
- [37] L. Xiong, Q. Deng, G.J. Tucker, D.L. McDowell, Y. Chen, Coarse-grained atomistic simulations of dislocations in Al, Ni and Cu crystals, Int. J. Plast. 38 (2012) 86–101.
- [38] L. Xiong, D.L. McDowell, Y. Chen, Nucleation and growth of dislocation loops in Cu, Al and Si by a concurrent atomistic-continuum method, Scr. Mater. 67 (2012) 633–636.
- [39] S. Xu, L. Xiong, Y. Chen, D.L. McDowell, Edge dislocations bowing out from a row of collinear obstacles in Al, Scr. Mater. 123 (2016) 135–139.
- [40] S. Xu, L. Xiong, Y. Chen, D.L. McDowell, An analysis of key characteristics of the Frank-Read source process in FCC metals, J. Mech. Phys. Solids 96 (2016) 460-476
- [41] S. Xu, L. Xiong, Y. Chen, D.L. McDowell, Sequential slip transfer of mixed-character dislocations across Σ3 coherent twin boundary in FCC metals: a concurrent atomistic-continuum study, npj Comput. Mater. 2 (2016) 15016.
- [42] L. Xiong, S. Xu, D.L. McDowell, Y. Chen, Concurrent atomistic-continuum simulations of dislocation-void interactions in fcc crystals, Int. J. Plast. 65 (2015) 33–42.
- [43] S. Xu, L. Xiong, Y. Chen, D.L. McDowell, Shear stress-and line length-dependent screw dislocation cross-slip in FCC Ni, Acta Mater. 122 (2017) 412–419.
- [44] S. Xu, L. Xiong, Y. Chen, D.L. McDowell, Validation of the Concurrent Atomistic-Continuum Method on Screw Dislocation/Stacking Fault Interactions, cryst. 7 (2017) 120.
- [45] S. Yang, Y. Chen, Multiscale Materials Modeling for Nanomechanics, Springer International Publishing, 2016, pp. 261–296.
- [46] S. Yang, Y. Chen, Concurrent atomistic and continuum simulation of bi-crystal strontium titanate with tilt grain boundary, Proc. R. Soc. A 471 (2015).
- [47] S. Yang, N. Zhang, Y. Chen, Concurrent atomistic-continuum simulation of polycrystalline strontium titanate, Philos. Mag. 95 (2015) 2697–2716.
- [48] X. Chen, L. Xiong, D.L. McDowell, Y. Chen, Effects of phonons on mobility of dislocations and dislocation arrays, Scr. Mater. 137 (2017) 22–26, https://doi.org/ 10.1016/j.scriptamat.2017.04.033.

- [49] L. Xiong, D.L. McDowell, Y. Chen, Sub-THz Phonon drag on dislocations by coarsegrained atomistic simulations, Int. J. Plast. 55 (2014) 268–278.
- [50] Y. Li, et al., Resonant interaction between phonons and PbTe/PbSe (001) misfit dislocation networks, Acta Mater. (2022), 118143.
- [51] X. Chen, et al., Ballistic-diffusive phonon heat transport across grain boundaries, Acta Mater. 136 (2017) 355–365, https://doi.org/10.1016/j.actamat.2017.06.054.
- [52] Y. Li, A. Diaz, X. Chen, D.L. McDowell, Y. Chen, Interference, scattering, and transmission of acoustic phonons in Si phononic crystals, Acta Mater. 224 (2022), 117481
- [53] T.C. Harman, P.J. Taylor, D.L. Spears, M.P. Walsh, Thermoelectric quantum-dot superlattices with high ZT, J. Electron. Mater. 29 (2000) L1–L2.
- [54] T.C. Harman, P.J. Taylor, M.P. Walsh, B.E. LaForge, Quantum dot superlattice thermoelectric materials and devices, Science 297 (2002) 2229–2232.
- [55] D.L. Partin, Lead salt quantum effect structures, IEEE J. Quantum Electron. 24
- [56] Z. Feit, M. McDonald, R.J. Woods, V. Archambault, P. Mak, Low threshold PbEuSeTe/PbTe separate confinement buried heterostructure diode lasers, Appl. Phys. Lett. 68 (1996) 738–740.
- [57] Y. Li, Z. Fan, W. Li, D.L. McDowell, Y. Chen, A multiscale study of misfit dislocations in PbTe/PbSe (001) heteroepitaxy, J. Mater. Res. (2019) 1–9.
- [58] K. Wiesauer, G. Springholz, Critical thickness and strain relaxation in high-misfit heteroepitaxial systems: PbTe 1– x Se x on PbSe (001), Phys. Rev. B 69 (2004), 245313
- [59] K. Wiesauer, G. Springholz, Near-equilibrium strain relaxation and misfit dislocation interactions in PbTe on PbSe (001) heteroepitaxy, Appl. Phys. Lett. 83 (2003) 5160–5162.
- [60] K. Wiesauer, G. Springholz, Strain relaxation and dislocation patterning in PbTe/ PbSe (001) lattice-mismatched heteroepitaxy, Appl. Surf. Sci. 188 (2002) 49–54.
- [61] G. Springholz, K. Wiesauer, Nanoscale dislocation patterning in PbTe/PbSe (001) lattice-mismatched heteroepitaxy, Phys. Rev. Lett. 88 (2001), 015507.
- [62] A. Raab, G. Springholz, Oswald ripening and shape transitions of self-assembled PbSe quantum dots on PbTe (111) during annealing, Appl. Phys. Lett. 77 (2000) 2991–2993.

- [63] M. Pinczolits, G. Springholz, G. Bauer, Direct formation of self-assembled quantum dots under tensile strain by heteroepitaxy of PbSe on PbTe (111), Appl. Phys. Lett. 73 (1998) 250–252.
- [64] K. Takayanagi, K. Kobayashi, K. Yagi, G. Honjo, Heteroepitaxy of chalcogenite compounds I. Misfit dislocation formation in monolayer overgrowths, Thin. Solid. Films 21 (1974) 325–339.
- [65] N. Hew, D. Spagnoli, L. Faraone, Molecular Dynamics Study of Heteroepitaxial Growth of HgCdTe on Perfect and Dislocated (211) B CdZnTe Substrates, ACS Appl. Electron. Mater. 3 (2021) 5102–5113.
- [66] X.W. Zhou, et al., Stillinger-weber potential for the II-VI elements zn-cd-hg-S-se-te, Phys. Rev. B 88 (2013), 085309.
- [67] C.J. Fennell, J.D. Gezelter, Is the Ewald summation still necessary? Pairwise alternatives to the accepted standard for long-range electrostatics, J. Chem. Phys. 124 (2006), 234104.
- [68] Z. Fan, et al., A transferable force field for CdS-CdSe-PbS-PbSe solid systems, J. Chem. Phys. 141 (2014), 244503.
- [69] A. Stukowski, K. Albe, Extracting dislocations and non-dislocation crystal defects from atomistic simulation data, Modell. Simul. Mater. Sci. Eng. 18 (2010), 085001.
- [70] H. Gao, Some general properties of stress-driven surface evolution in a heteroepitaxial thin film structure, J. Mech. Phys. Solids 42 (1994) 741–772
- [71] P. Müller, et al., Reduction of threading dislocation densities in heavily lattice mismatched PbSe on Si (111) by glide, Phys. Rev. Lett. 78 (1997) 3007.
- [72] H. Zogg, et al., Thermal-mismatch strain relaxation mechanisms in heteroepitaxial lead chalcogenide layers on Si substrates, Semicond. Sci. Technol. 8 (1993) S337.
- [73] D. Eaglesham, M. Cerullo, Dislocation-free stranski-krastanow growth of Ge on Si (100), Phys. Rev. Lett. 64 (1990) 1943.
- [74] G. Springholz, A.Y. Ueta, N. Frank, G. Bauer, Spiral growth and threading dislocations for molecular beam epitaxy of PbTe on BaF2 (111) studied by scanning tunneling microscopy, Appl. Phys. Lett. 69 (1996) 2822–2824.
- [75] Y.N. Osetsky, D.J. Bacon, An atomic-level model for studying the dynamics of edge dislocations in metals, Modell. Simul. Mater. Sci. Eng. 11 (2003) 427.
- [76] T. Zhu, C.-Y Wang, Misfit dislocation networks in the γ/γ' phase interface of a Ni-based single-crystal superalloy: Molecular dynamics simulations, Phys. Rev. B 72 (2005), 014111.